C-V profiling of ultra-shallow junctions using a buried layer with stepped doping

Cuiqin Xu

Supervisors:

Miloš Popadić

Prof. L. K. Nanver

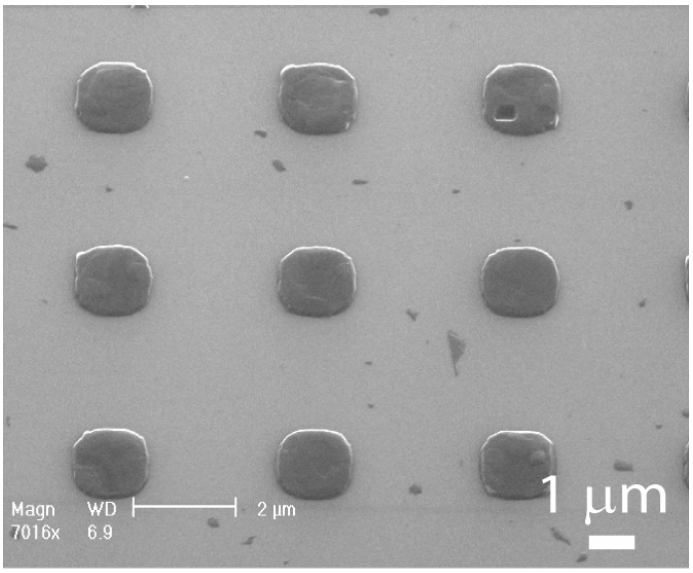

Delft Institute of Microsystems and Nanoelectronics
Department of Microelectronics
Faculty of Electrical Engineering, Mathematics and Computer Science
Delft University of Technology
Delft, The Netherlands

1 Introduction

1.1 Background

In order to improve the performance and speed of integrated circuits, reduce the cost per transistor, dimensions of MOSFETs have been shrunk continuously [1, 2]. However with the downscaling of gate length, ultra-shallow source and drain junctions are necessary to suppress the short channel effect [3].

According to the International Technology Roadmap for semiconductors (ITRS), the S/D junction depth should be smaller than 10 nm to minimize the short channel effect [4]. On the other hand, in order to reduce the S/D contact resistance and parasitic resistance, high electrically active doping concentration and high doping abruptness at the S/D-extension to channel junction are required [5, 6].

So the formation and characterization of ultra-shallow junction become crucial for future device fabrication [7, 8]. The performance of device is tightly dependent on the doping profiles of the S/D doping profiles. A high active doping concentration at the surface reduces the contact resistance. Both accumulation and sheet resistance will be minimum for a given activation level when the junction profile is abrupt, box-like, with nearly constant doping from surface to junction [8]. It is very important and challenging to measure the activated doping level and its distribution through the ultra-shallow junction because of the stringent depth resolution and quantitative accuracy requirements.

1.2 Conventional profiling techniques

There are many different kinds of profiling techniques, such as secondary ion mass spectrometry (SIMS), electrochemical capacitance-voltage profiling (ECV), spreading resistance profiling (SRP), Hall effect profiling, optical profiling, Rutherford backscattering and differential capacitance-voltage profiling. Each technique has its own advantages and disadvantages [9].

Secondary ion mass spectrometry (SIMS) technique is attractive for the high spatial resolution and can be used for any semiconductor. It offers good detection sensitivity but not as high as electrical or optical methods. The disadvantage is that it is destructive and the knock-on effect reduces the depth resolution of SIMS profiling, on the other hand it tells the chemical impurity density instead of electrically active

doping concentration. What is more, it requires rather complex and expensive equipment.

Electrochemical capacitance-voltage technique has no depth limit and good sensitivity but it is destructive. Also errors can be caused by the inaccurate measurement of the area of the electrolyte Silicon contact and etched depth [7, 9].

Spreading resistance technique is a routine method for generating profiles which is capable of profiling through an arbitrary number of p-n junctions. Also, it has a very high dynamic range (10^{12}–10^{21} cm^{-3}), no depth limitation and no destruction to the sample. However, it requires complex sample preparation and data analysis, and the profiling accuracy is dependent on the setting of carrier mobility in data analysis [9].

Hall Effect can provide the average value of the carrier density and the carrier mobility but it is not suitable for the measurement of the doping concentration and the doping gradient of an ultra-shallow junction [9].

The major advantages of Optical techniques lie in the high sensitivity and the fact that it is contactless and nondestructive. However, special equipment is necessary and accurate profiling is impossible since only the average value of the doping concentration is obtained [9].

Rutherford backscattering (RBS) is a non-destructive, quantitative technique requiring no standards. It is most useful for heavy elements in a light matrix. The disadvantage of RBS is the low sensitivity and the requirement of specialized equipment not readily available in most semiconductor laboratories. Also, it is difficult to measure light elements [9].

As conventional differential capacitance-voltage method is concerned, it is very attractive due to the high sensitivity and accuracy, and simple data processing. Also it is nondestructive and experimentally simple. However, the profiling depth is limited by the breakdown voltage at reverse bias, and the zero-bias space charge region width [9]. The most serious disadvantage of conventional differential capacitance-voltage profiling technique is that it can only be applied for the profiling of a low doped region of asymmetrical junctions, i.e., p^+-n or n^+-p junctions where one side of the junction is substantially more highly doped than the other side [9].

Conventional capacitance-voltage method is not suitable for the doping profiling of the highly doped region of an asymmetrical junction. It has been proposed that if the doping profile on one side of the junction is known, then the profile on the other side can be extracted from the *C-V* relationship of the junction [11]. However, the method has not been used experimentally and the formulas proposed in [11] are dependent on

the relationship between the capacitance and the total voltage drop across the junction which includes the built-in voltage and is not possible to measure experimentally.

In summary, none of the profiling techniques discussed is perfect to offer all the advantages of high sensitivity, high depth resolution, being non-destructive, etc.

1.3 This thesis

The goal of this thesis is to develop a novel *C-V* profiling structures that enables the extraction of the doping profiles of the highly doped (e.g. p^+) region of an ultra-shallow (e.g. p^+-n) diode. In this thesis, expressions are derived for the evaluation of the doping profile in the p region based on the knowledge of the relationship between the capacitance and the reverse applied voltage and the doping profile in the n region. This is possible only with the accurate knowledge of x_{n0} which stands for the coordinate of the boundary of the depletion region of the n region at thermal equilibrium. We have designed a special doping profile in the n region for the accurate estimation of x_{n0} which is an crucial parameter for the exact extraction of the doping profile in the p^+ region.

In this thesis, different profiling structures are considered and their capacitance versus the reverse applied voltage relationships are obtained by two different ways: analytical calculations and Medici simulations. The structure of choice is currently being fabricated.

In analytical calculations, for a known p^+-n junction, with depletion approximation, the capacitance versus applied voltage relationship of a p^+-n junction is calculated by solving the Poisson's equation. Then based on the known doping profile on the n side and the analytically computed $C(V_R)$ relationship, the doping profile on the p side is extracted with different assumption of x_{n0}. It is shown that with stepped doping profiles in the n region, x_{n0} and consequently the doping profiles in the p region can be computed exactly. On the other hand, with uniformly doped n region, only the abruptness of the doping profile in the p region can be accurately calculated.

However, the analytical-calculated $C(V_R)$ data cannot exactly present the real *C-V* relationship of device. In the analytical calculation, the depletion approximation is made and only the Poisson's equation is solved, however, the real distribution of carriers and characteristics of device is determined not only by the Poisson's equation but also by the continuity equation and transport equations of carriers. In order to get a more realistic *C-V* characteristic of the device, Medici simulations of p^+-n junctions are carried out by solving the Poisson's equation, the continuity equation and the transport equations of carriers.

In Medici simulations, the $C(V_R)$ relationships of both the p^+-n junction and the n-Schottky junction with the same step-like n profile are simulated. The doping profile in the n region is computed based on the $C(V_R)$ relationship of the Schottky diode. The depletion region edge (x_{n0}) is estimated and it is proven that the accuracy of the x_{n0} estimation can be controlled within 1 nm. In the end, with doping profiles in the n region, $C(V_R)$ relationship of p^+-n junction and accurate evaluation of x_{n0}, the doping profile in the p^+ doped region is successfully calculated and fits very well with the Medici simulation results. So it is proven that the two sided profiling method can be used for accurate profiling of the highly doped and abrupt p region of p^+-n junction with stepped doping in the n region.

Also, evaluation of the doping profile in the p^+ region of a p^+-n junction with a uniformly doped n region is discussed in detail, and it is shown that the doping gradient in the p region can be calculated independently from the assumption of x_{n0}.

1.4 Organization of this thesis

In Chapter 1, the background for this thesis is introduced, both the advantages and disadvantages of different profiling techniques are discussed. The motivation and the outline of this thesis are explained.

In Chapter 2, the theory background of the *C-V* profiling is discussed and the expressions of *C-V* profiling of a two-sided junction are derived. Also *C-V* profiling of a Schottky diode is discussed.

In Chapter 3, based on the analytical calculation of the $C(V_R)$ relationship of a p^+-n junction under depletion approximation, the novel *C-V* profiling method is applied for the profiling of the p^+ region.

In Chapter 4, based on the Taurus Medici simulated $C(V_R)$ relationships of the p^+-n and the n-Schottky diodes with the same n profile, the doping profile in the n region is calculated and the novel *C-V* profiling method is applied for the profiling of the p^+ region.

Besides the work discussed from Chapter 1 to Chapter 4, the author has been involved with a project about the extraction of minority carrier lifetime and surface recombination velocity of Al-doped solid phase epitaxy (SPE) ultra-shallow p^+-n Junctions which is discussed in Chapter 5. Firstly, based on the *I-V* characteristic of 6 devices with different emitter sizes, using the geometric scaling rule, linear fitting is applied to extract the area current density of the collector and the base current of a

p^+-n-p BJT with Al-doped SPE emitter. Then, 1-D Tsuprem4 and Medici simulations of the p^+-n-p BJT are carried out, and the minority carrier lifetime and surface recombination velocity are modulated to get good fitting between the simulated collector and base current density and the extracted area current density of the collector and the base current.

References

[1] H.-S. Wong, D. J. Frank, P. M. Solomon, H.-J. C. Wann, and J. Welser, "Nanoscale CMOS," Proc. IEEE, vol. 87, pp. 537–570, 1999.

[2] G. E. Moore, "Cramming more components on to integrated circuits", Electronics, Vol. 38, no. 8, April 19, 1965; "Progress in digital integrated electronics", IEDM Tech Dig. pp.11-13, 1975.

[3] Hajime Kurata and Toshihiro Sugii, "Impact of Shallow Source/Drain on the Short-Channel Characteristics of pMOSFET's ", IEEE ELECTRON DEVICE LETTERS, VOL. 20, NO. 2, FEBRUARY 1999

[4] "International technology roadmap for semiconductors (ITRS)", 2007. [Online]. http://www.itrs.net/Links/2007ITRS/Home2007.htm

[5] F. Sarubbi, L. K. Nanver, and T. L. M. Scholtes, "CVD delta-doped boron surface layers for ultra-shallow junction formation," in Advanced Gate Stack, Source/Drain, and Channel Engineering for Si-Based CMOS 2: New Materials, Processes, and Equipment, 210th Meeting of The Electrochemical Society, Cancun, Mexico, October 29-November 3, 2006, ECS Transactions, vol. 3, no. 2, pp. 35–44.

[6] Mikael Östling, Bengt Gunnar Malm, Martin von Haartman, Julius H°allstedt, Zhen Zhang,Per-Erik Hellström, and Shili Zhang, "Challenges for 10 nm MOSFET process integration", Journal of Telecommunications and Information Technology, 2007

[7] Hui-Zhen Wu , Guo-Ping Ru,Jin, C.G. Mizuno, B Mizuno2, Yu-Long Jiang, Xin-Ping Qu,Bing-Zong Li, "ECV Profiling of Ultra-Shallow Junction Formed by Plasma Doping", Proc. IEEE-IWJT, pp. 120-122, Shanghai, China, 2006 IEEE press, ISBN 1-4244-0047-3

[8] E.C. Jones and E. Ishida," Shallow junction doping technologies for ULSI", Mater. Sci. Eng. R 24 (1998)

[9] D. K. Schroder, Semiconductor Material and Device Characterization,2nd ed. New York, USA: John Wiley and Sons,1998.

[10] P. C. Zalm, J. Vriezema, D. J. Gravesteijn, G. F. A. van de Walle and W. B. de Boer,Surf . Interface Anal . 17, 556 (1991)

[11] H. J. J. De Man. On the Calculation of Doping Profile from C (V) Measurement on Two-sided Junctions. IEEE Transactions on Electron Devices, 1970, December, Vol. 17:1087

2 Differential capacitance of a p-n junction and a Schottky diode

In this chapter, the basic theory of the differential capacitances of a p-n junction and a Schottky diode is discussed. Also, expressions are derived for the profiling of p side based on the profile on the n side and the $C(V_R)$ relationship of the p-n junction.

2.1 Differential capacitance of a p-n diode

The capacitance-voltage profiling technique is widely used and relies on the fact that the width of depletion region of p-n diode depends on the applied voltage [3]. In order to get a good understanding of *C-V* profiling, in this section, the theory background of the differential capacitance of a p-n junction is discussed in detail.

2.1.1 Thermal equilibrium state

At thermal equilibrium state, the Fermi energy level through a p-n junction is constant. For simplicity, a step p-n junction is considered, in which the p region is uniformly doped at N_a and the n region is uniformly doped at N_d. As shown in Figure 2.1, there is a barrier between the p region and the n region which is called the built-in potential barrier V_{bi}. The built-in potential barrier is the difference between the intrinsic Fermi-levels in the p and n regions and essentially determined by the doping profiles. The built-in potential barrier for step junction can be expressed by the following equation

$$V_{bi} = \frac{kT}{e} \ln\left(\frac{N_a N_d}{n_i^2}\right) \tag{2.1}$$

In equation (2.1), the parameter e represents the elementary charge, k is the Boltzmann's constant, T is the temperature, and n_i is the intrinsic concentration of electrons [1,2].

删除的内容: (2.1)

However, the built-in potential barrier of a p-n junction cannot be measured by voltmeter since new potential barriers will be formed between the probe and the semiconductor which will cancel V_{bi} .

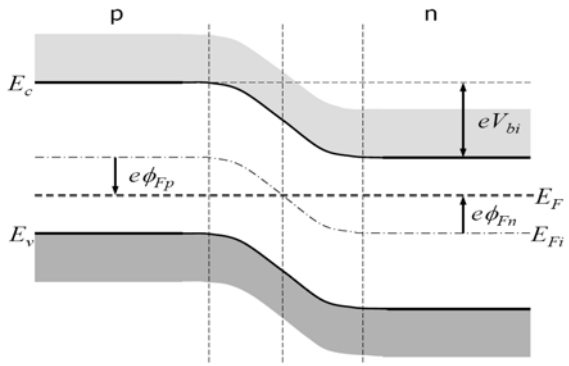

Figure 2.1 Energy-band diagram of a step-like p-n junction in thermal equilibrium [1].

2.1.2 Electric field and the total potential drop

As a result of the separation of positive and negative charges, an electric filed is generated in the depletion region. The electric field and the potential barrier through the depletion region are determined by the Poisson's equation [1, 2]. For simplicity, we take a one-dimensional analysis for example.

$$\frac{d^2\phi(x)}{dx^2} = -\frac{\rho(x)}{\varepsilon_S} = -\frac{dE(x)}{dx} \tag{2.2}$$

In equation (2.2), $\phi(x)$ is the electric potential, $\rho(x)$ is volume charge density as function of position, ε_s is the permittivity of the semiconductor, and $E(x)$ is the electric field. For an arbitrarily doped p-n junction, assuming that all dopant atoms are electrically active, the net charge can be expressed by equation (2.3).

删除的内容: (2.2)

删除的内容: (2.3)

$$\rho(x) = e\left(N_d(x) - n(x) - N_a(x) + p(x)\right) \tag{2.3}$$

where $n(x)$ is the electron concentration and $p(x)$ is the hole concentration.

The electric field can be calculated by integrating equation (2.3),

删除的内容: (2.3)

$$E = \int \frac{\rho(x)}{\varepsilon_S} dx \tag{2.4}$$

To solve this equation, boundary conditions of electric field should be considered. The semiconductor is electrically neutral outside the depletion region, and the electric field equals zero in the neutral p and n regions. So the electric fields at the boundaries of the depletion region are 0.

Defining the potential on the edge of the depletion region near the neutral p region is 0 and integrating the electric field, the total potential drop across the p-n junction can

be calculated as

$$V = -\int E(x)dx \tag{2.5}$$

2.1.3 Reverse bias

When a positive voltage is applied to the n region with respect to the p region, the Fermi energy level (E_F) in the p region is different from that in the n region. As shown in figure 2.2, under reverse bias, the total potential barrier across the p region and the n region increases. The total potential across the junction, V_T, is the sum of the built-in potential under thermal equilibrium and the reverse applied voltage

$$V_T = V_{bi} + V_R \tag{2.6}$$

where V_R represents the reverse applied voltage.

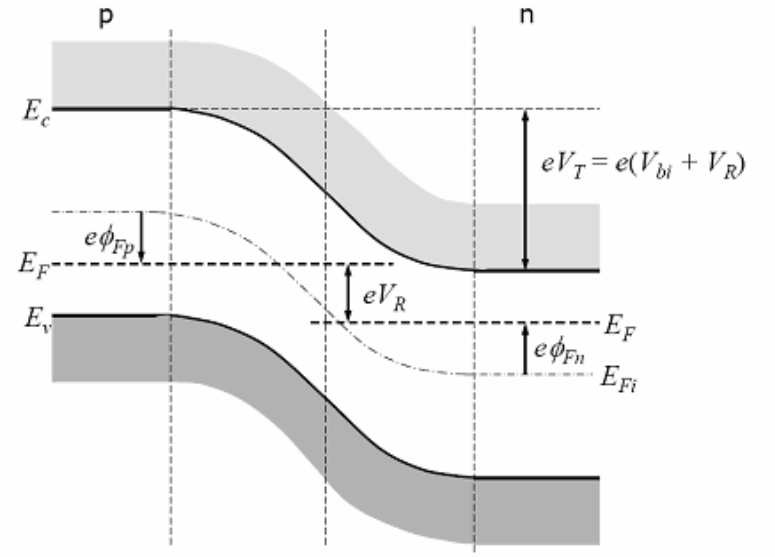

Figure 2.2 Energy band diagram of a p-n junction under reverse bias [1].

2.1.4 Junction capacitance

If the reverse biased voltage of a p-n junction increases, both the positive charges and negative charges in the depletion region will increase. Since the system is charge neutral, the increased positive and negative charges are equal, as shown in Figure 2.3.

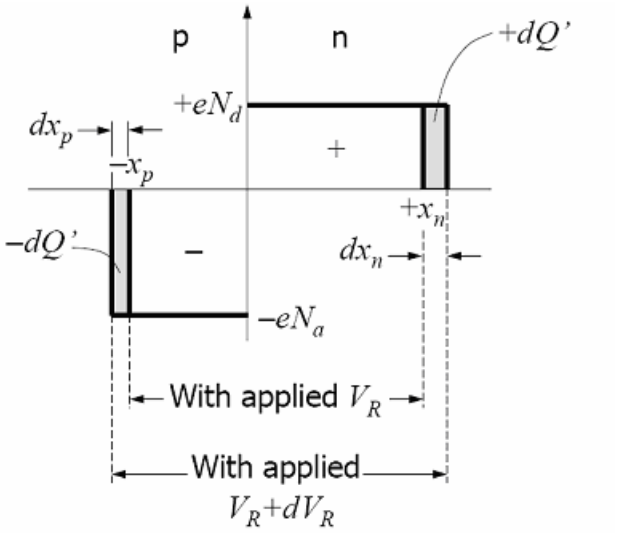

Figure 2.3 Differential change of the space charge width with a differential change in reverse-bias voltage for a uniformly doped p-n junction [1].

The differential capacitance is defined as

$$C_j' = \frac{dQ'}{dV_R} = \frac{dQ'}{W\dfrac{dQ'}{\varepsilon_s}} = \frac{\varepsilon_s}{W} \tag{2.7}$$

C_j' is defined as junction capacitance per unit area which is, the differential charge dQ' is the change of quantity of charge per unit area. If the area of the p-n junction is A, then the capacitance of the whole junction can be written as

$$C = \frac{A\varepsilon_s}{W} \tag{2.8}$$

Since the space charge width is a function of the reverse bias, the capacitance of the junction is also a function of the reverse bias voltage. For an arbitrarily doped p-n junction, the analytical calculation of differential capacitance versus applied voltage will be discussed in Chapter 3.

2.2 *C-V* profiling of a p-n junction

In this section, expressions are derived for profiling on one side of a p-n junction, based on the doping profile on the other side and the $C(V_R)$ relationship of the p-n junction. It is shown that for a p-n junction, if the doping profile on one side is known, then making use of the capacitance voltage measurement results, with the knowledge of the position of the edge of depletion region, the doping profile on the other side can be uniquely determined.

2.2.1 *C-V* profiling of a p-n junction

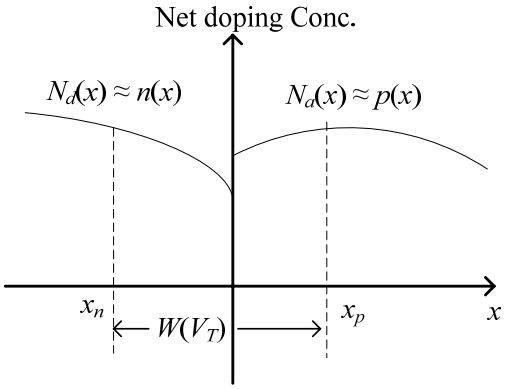

Figure 2.4 Definitions of an arbitrarily doped p-n junction [4].

An arbitrarily doped p-n junction is shown in Figure 2.4, $N_d(x)$ represents the donor concentration in the region where $x < 0$, $N_a(x)$ represents the acceptor profile in the region where $x > 0$, $W(V_T)$ is the width of the depletion region when the total potential drop through the junction equals V_T, and x_n and x_p stand for the edges of the depletion region to the neutral n and p regions respectively [4].

With depletion approximation [4]-[6], it is assumed that the carriers are completely depleted in the depletion region, and the region outside the depletion region is charge neutral. Then, the electric field through the junction can be expressed by integrating the Poisson's equation.

$$E(x) = \frac{e}{\varepsilon_s}\int_{x_n}^{x} N_d(x)dx \qquad \text{for } x < 0 \qquad (2.9)$$

$$E(x) = \frac{e}{\varepsilon_s}\left[\int_{x_n}^{0} N_d(x)dx + \int_{0}^{x} -N_a(x)dx\right] \qquad \text{for } x > 0 \qquad (2.10)$$

Under depletion approximation, the electric field is assumed to be zero in the neutral p region for $x > x_p$, therefore

$$E(x_p) = \int_{x_n}^{0} N_d(x)dx + \int_{0}^{x_p} -N_a(x)dx = 0 \qquad (2.11)$$

Equation (2.11) can be written in the differential form

删除的内容: (2.11)

$$N_d(x_n)dx_n = -N_a(x_p)dx_p \qquad (2.12)$$

Equation (2.12) is consistent with the charge neutrality of the whole p-n junction system. Integrating the electric field through the depletion region, the total potential

删除的内容: (2.12)

barrier between the neutral p and n regions is given by

$$V_T = \int_{x_n}^{x_p} E(x) = \frac{e}{\varepsilon_s}\left\{\int_{x_n}^{0}\left[\int_{x_n}^{x} N_d(u)du\right]dx + \int_{0}^{x_p}\left[\int_{x_n}^{0} N_d(u)du + \int_{0}^{x} -N_a(u)du\right]dx\right\} \tag{2.13}$$

From equation (2.13) we obtain

$$dV_T = -\frac{e}{\varepsilon_s}[x_n N_d(x_n)dx_n + x_p N_a(x_p)dx_p] \tag{2.14}$$

Combining equations (2.12) and (2.14), dx_n and dx_p can be expressed as

$$dx_n = -\frac{\varepsilon_s dV_T}{eW(V_T)N_d(x_n)} \tag{2.15}$$

$$dx_p = \frac{\varepsilon_s dV_T}{eW(V_T)N_a(x_p)} \tag{2.16}$$

As shown in Figure 2.4, the width of the depletion region is defined by

$$W(V_T) = x_p(V_T) - x_n(V_T) \tag{2.17}$$

Then in the differential form, it is found that

$$dW = \frac{dW}{dV_T}dV_T = dx_p - dx_n \tag{2.18}$$

The combination of equations (2.15), (2.16) and (2.18) gives

$$\frac{1}{N_d(x_n)} + \frac{1}{N_a(x_p)} = \frac{e}{\varepsilon_s}W(V_T)\frac{dW}{dV} \tag{2.19}$$

Equation (2.19) can be written as

$$N_a(x_p) = -\frac{N_d(x_n)}{1 - \frac{e}{\varepsilon_s}W(V_T)\frac{dW}{dV}N_d(x_n)} \tag{2.20}$$

Integrating equation (2.15) yields

$$\int_0^{x_n} N_d(x_n)dx_n = -\frac{\varepsilon_s}{e}\int_0^{V}\frac{dV_T}{W(V_T)} \tag{2.21}$$

If the p-n junction is unbiased, the junction is at thermal equilibrium and the total potential barrier is equal to the built-in potential, that is

$$V_T = V_{bi} \quad \text{at thermal equilibrium} \tag{2.22}$$

删除的内容: (2.13)
删除的内容: (2.12)
删除的内容: (2.14)
删除的内容: (2.15)
删除的内容: (2.16)
删除的内容: (2.18)
删除的内容: (2.19)
删除的内容: (2.15)

Supposing that at thermal equilibrium the edge of the depletion region to the neutral n region is located at x_{n0}, equation (2.21) can be written as

$$\int_0^{x_{n0}} N_d(x_n)dx_n = -\frac{\varepsilon_s}{e}\int_0^{V_{bi}} \frac{dV_T}{W(V_T)} \tag{2.23}$$

With a certain reverse bias voltage applied, as shown in equation (2.6), V_T is the sum of the built-in potential under thermal equilibrium and the applied voltage, so

$$\int_0^{x_n} N_d(x_n)dx_n = -\frac{\varepsilon_s}{e}\left\{\int_0^{V_{bi}} \frac{d(V_T)}{W(V_T)} + \int_{V_{bi}}^{V_{bi}+V_R} \frac{d(V_T)}{W(V_T)}\right\} \tag{2.24}$$

What is more, for a specific p-n junction, the built-in potential of the junction is constant, then

$$\frac{d(V_T)}{W(V_T)} = \frac{d(V_R)}{W(V_R)} \tag{2.25}$$

Then, combining equations (2.23), (2.24) and (2.25), it is found that

$$\int_{x_{n0}}^{x_n} N_d(x_n)dx_n = -\frac{\varepsilon_s}{e}\int_0^{V_R} \frac{dV_R}{W(V_R)} \tag{2.26}$$

Substituting equation (2.8) into equation (2.26) gives,

$$\int_{x_{n0}}^{x_n} N_d(x_n)dx_n = -\frac{1}{eA}\int_0^{V_R} C(V_R)dV_R \tag{2.27}$$

Since V_{bi} is constant, equations (2.17) and (2.20) can also be written as

$$W(V_R) = x_p(V_R) - x_n(V_R) \tag{2.28}$$

$$N_a(x_p) = -\frac{N_d(x_n)}{1 - \frac{e}{\varepsilon_s}W(V_R)\frac{dW}{dV_R}N_d(x_n)} \tag{2.29}$$

Based on the measured $C(V_R)$ relationship of the p-n junction, using equation (2.8), $W(V_R)$ can be obtained. Then, with the knowledge of x_{n0} and the knowledge of the doping profile in the n region, using equation (2.27), $x_{n\_esti}(V_R)$ which stands for the estimated relationship between x_n and V_R can be calculated. Using equation (2.28), the estimated x_p versus V_R relationship, $x_{p\_esti}(V_R)$, can be computed based on the knowledge of $x_{n\_esti}(V_R)$ and $W(V_R)$. Finally, $N_a(x_p)$ can be obtained from equation (2.29). During this process, x_{n0} is an important parameter, however, generally speaking, the value of x_{n0} is not known. In this thesis, it is found that for a p-n junction with a step-like n profile, the value of x_{n0} can be accurately estimated. The detailed process will be introduced in Chapter 3.

We can come to the conclusion that theoretically speaking, as a p^+-n junction is concerned, the doping profiles in the highly doped p region can be calculated,

删除的内容: (2.21)
删除的内容: (2.6)
删除的内容: (2.23)
删除的内容: (2.24)
删除的内容: (2.25)
删除的内容: (2.8)
删除的内容: (2.26)
删除的内容: (2.17)
删除的内容: (2.20)
删除的内容: (2.8)
删除的内容: (2.27)
删除的内容: (2.28)
删除的内容: (2.29)

provided the knowledge of the doping profile in the n region, the $C(V_R)$ relationship of the junction and the knowledge of x_{n0}.

2.2.2 Conventional *C-V* profiling of a highly asymmetrical junction

The conventional *C-V* profiling technique can be successfully used for the profiling of the low doped side of p^+-n or n^+-p junctions. If the doping profile on the highly doped side is orders of magnitude higher than that on the low doped side, then the spreading of depletion region into the highly doped region can be neglected [3]. The standard equations for one-sided *C-V* profiling are

$$W = \frac{\varepsilon_S A}{C} \tag{2.30}$$

$$N_B(W) = \frac{2}{e\varepsilon_S A^2 d\left(1/C^2\right)/dV_R} \tag{2.31}$$

where N_B is the doping profile in the low doped region [3].

The conventional *C-V* profiling of one-sided junction is a special case of the two-sided profiling technique. If $N_d(x)$ is several orders of magnitude higher than $N_a(x)$, the junction becomes one-sided, then we can assume that x_n is always zero under any bias, so from equation (2.17), x_p is equal to the width of depletion region, equation (2.29) can be written as

$$N_a(x_p) = N_a(W) = -\frac{\varepsilon_s}{eW(V_R)}\left(\frac{dW}{dV_R}\right)^{-1} \tag{2.32}$$

$$d\left(\frac{1}{C^2}\right)/dV_R = -\left(\frac{2}{C^3}\right)dC/dV_R \tag{2.33}$$

Combined with equation (2.8), using the identity expressed by equation (2.33), equation (2.32) can be written as

$$N_a(W) = -\frac{C^3}{e\varepsilon_s A^2 dC/dV_R} = \frac{2}{e\varepsilon_s A^2 d\left(1/C^2\right)/dV_R} \tag{2.34}$$

which is in accordance with equation (2.31).

删除的内容: (2.17)

删除的内容: (2.29)

删除的内容: (2.8)

删除的内容: (2.33)

删除的内容: (2.32)

删除的内容: (2.31)

2.3 Differential capacitance and *C-V* profiling of a Schottky diode

A schematical representation of the energy-band diagram of an n-Schottky diode is shown in Figure 2.5. If the work function of metal is larger than that of semiconductor,

after the contact between metal and semiconductor, electrons tend to move from semiconductor to the metal until reaching thermal equilibrium state in which the Fermi level is constant through the system as indicated in Figure2.5 (a).

As shown in Figure 2.5 (b), if the n-Schottky diode is reverse biased, the potential drop and electric field across the depletion layer increase, more electrons in the semiconductor will be depleted.

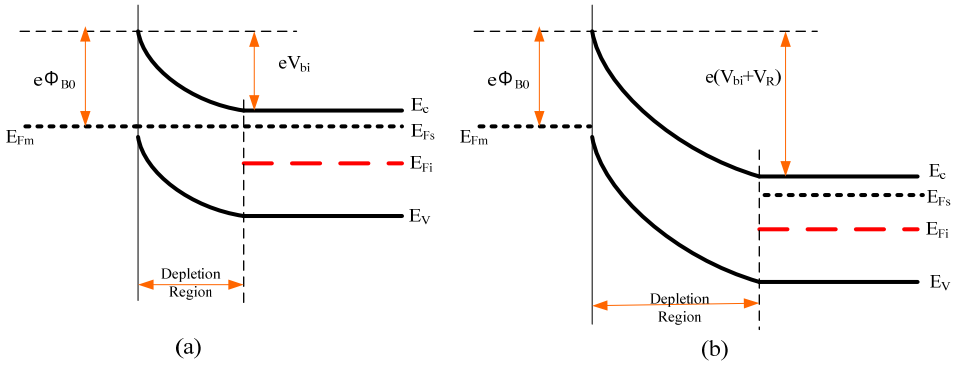

Figure2.5 Energy-band diagram of an n-Schottky diode (a) at thermal equilibrium (b) under reverse bias [1].

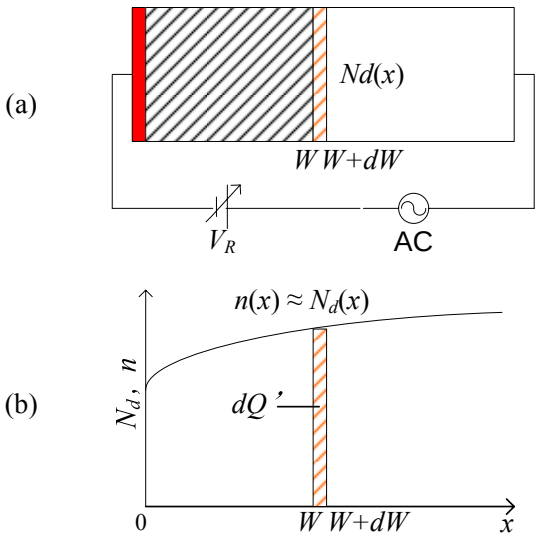

Figure.2.6 (a) A reverse-biased n-Schottky diode, (b) the doping density and the majority carrier density profiles in the depletion approximation [3].

A reverse biased Schottky diode is shown in Figure 2.6, the substrate is doped with donors. At a certain reverse DC bias V_R, the width of the depletion region is W.

Applying a high frequency, small amplitude sinusoidal AC signal, as the AC voltage increases from 0 to a positive value, more electrons are depleted, the increment of charge removed from the boundary of the depletion layer can be expressed by

$$dQ = eAN_d(W)dW \tag{2.35}$$

In equations (2.35) and (2.39), A is the area of the Schottky diode. Under a certain DC reverse bias V_R, the differential capacitance of Schottky diode is defined by

$$C = \frac{dQ}{dV_R} \tag{2.36}$$

Combining equation (2.35) and (2.36), the differential capacitance can be expressed by

$$C = \frac{dQ}{dV_R} = eAN_d(W)\frac{dW}{dV_R} \tag{2.37}$$

Considering the reverse-biased Schottky diode as a parallel capacitance, the capacitance of the Schottky diode can also be expressed by

$$C = \frac{\varepsilon_s A}{W} \tag{2.38}$$

Combining equation (2.37) and (2.38), the doping concentration can be expressed as

$$N_d(W) = -\frac{C^3}{e\varepsilon_s A^2 dC/dV_R} \tag{2.39}$$

Using the identity described by equation (2.33), the doping concentration at W can also be written as

$$N_d(W) = \frac{2}{e\varepsilon_s A^2 d\left(1/C^2\right)/dV_R} \tag{2.40}$$

As discussed in section 2.2, to obtain the doping profile in the highly doped p^+ region, the doping profiles in the n region is necessary. Experimentally, it is possible to fabricate n-Schottky diode and p^+-n junction with essentially the same n profiles. After that, based on the C-V measurement of the Schottky diode, the doping profiles in the n region of Schottky diode can be computed, thus the doping profiles in the n region of the p^+-n junction is obtained.

删除的内容: (2.35)

删除的内容: (2.35)

删除的内容: (2.36)

删除的内容: (2.37)

删除的内容: (2.38)

删除的内容: (2.33)

References

[1] Donald A.Neamen, Semiconductor Physics and Devices: Basic Principles, 3rd ed. New York, USA: McGraw-Hill, 2003.

[2] S.M.Sze, Semiconductor Devices: Physics and Technology, 2nd ed. New York, USA : Wiley, 2002

[3] D. K. Schroder, Semiconductor Material and Device Characterization, 2nd ed. New York, USA: John Wiley and Sons,1998.
[4] H. J. J. De Man. On the Calculation of Doping Profile from C (V) Measurement on Two-sided Junctions. IEEE Transactions on Electron Devices, 1970, December, Vol. 17:1087
[5] D. P. Kennedy, P. C. Murley, W. Kleinfelder, On the measurement of impurity atom distributions in silicon by the differential capacitance technique. IBM J. Res. Develop, 1968, Sept: 399
[6] Walter C. Johnson, Peter T. Panousis, The influence of Debye Length on the *C-V* Measurement of Doping Profiles. IEEE Transaction Devices, 1971, October, NO.10, vol. ED-18:965

3 Two-sided *C-V* profiling – analytical calculation

As discussed in Chapter 2, all the formulas for two-sided profiling of p-n junctions are derived under abrupt depletion approximation, and x_{n0} is an essential parameter in profiling non-highly-asymmetrical or two-sided p-n junctions. According to equations (2.27), (2.28) and (2.29), using a wrong value of x_{n0} in the calculations would result in a wrong calculation of $x_n(V_R)$, followed by the wrong calculation of $x_p(V_R)$ and $N_a(x_p)$. However, x_{n0} is not known.

删除的内容: (2.27)

删除的内容: (2.28)

删除的内容: (2.29)

In order to solve the problem that x_{n0} is not known, a p^+-n diode with stepped doping profile in the n region is designed. To test whether the designed structure is effective for the extraction of x_{n0}, $C(V_R)$ relationship is firstly analytically calculated under depletion approximation. Then, taking the analytically calculated $C(V_R)$ relationship in place of the measured $C(V_R)$ of a p^+-n diode, based on the known n doping profile, using equation (2.27), (2.28),and (2.29), with different assumptions of x_{n0}, different $x_n(V_R)$, $x_p(V_R)$ and $N_a(x_p)$ are calculated and compared to the known values. It is shown that with a stepped n doping profile, x_{n0} and the p doping profile can be exactly calculated.

删除的内容: (2.27)

删除的内容: (2.28)

删除的内容: (2.29)

3.1 Analytical calculation of $C(V_R)$ of an arbitrarily doped junction

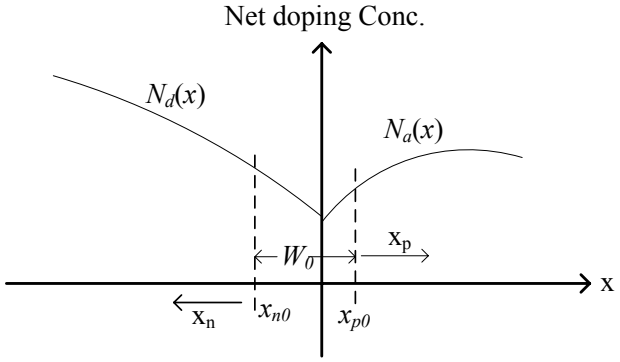

Figure 3.1 Schematic of an arbitrarily doped p-n junction. At thermal equilibrium the boundaries of depletion region are denoted as x_{n0} and x_{p0}. As reverse bias voltage

increases, the width of the depletion region increases as indicated by the arrows.

As discussed in Chapter 2, with depletion approximation it is assumed that the semiconductor is divided into two kinds of distinct regions, one fully depleted of charge carriers, and the other absolutely charge neutral. For an arbitrarily doped p-n junction as shown in Figure 3.1 the $C(V_R)$ relationship can be analytically calculated following the process discussed bellow.

First, based on the known p and n doping profiles, different couples of boundaries of depletion region near neutral p and n region can be calculated according to the charge neutrality at any bias. Second, with the knowledge of different couples of x_n and x_p, the corresponding total potential drop can be calculated using equation (2.13). Third, using equation (2.1) the built-in potential barrier corresponding to each couple of x_n and x_p can be computed and compared to the corresponding total potential drop. The couple of x_n and x_p where the built-in potential is equal to the total potential drop are defined as x_{n0} and x_{p0}, and the corresponding built-in potential barrier is defined as the built-in barrier of the p-n diode. Finally, using to equations (2.6), (2.28), and (2.8), the $C(V_R)$ relationship can be analytically calculated.

删除的内容: (2.13)

删除的内容: (2.1)

删除的内容: (2.6)

删除的内容: (2.28)

删除的内容: (2.8)

3.2 Profiling based on an analytical calculation

Using the two-sided profiling technique discussed in Chapter 2, based on the analytically calculated relationship between capacitance versus reverse applied voltage, taking the doping profile in the n region which has been used to calculate the analytical $C(V_R)$ relationship as known, the doping profiles in the p region can be successfully predicted with a right assumption of the boundary coordinates of depletion region at thermal equilibrium [3].

Using equation (2.8), the depletion width versus reverse applied voltage relationship can be calculated. Then, with an assumption of x_{n0}, $x_{n\_esti}(V_R)$ which stands for the estimated relationship between boundary of depletion region near the neutral n region and the reverse applied voltage, can be calculated using equation (2.27). Then, $x_{p\_esti}(V_R)$ can be computed using equation (2.17). In the end, using equation (2.29), the doping profile in the p region is obtained.

删除的内容: (2.8)

删除的内容: (2.27)

删除的内容: (2.17)

删除的内容: (2.29)

3.3 Analytical calculation of $C(V_R)$ and profiling based on $C(V_R)$

Based on the two-sided profiling technique discussed in Chapter 2 and section 3.1, the

analytical calculations of $C(V_R)$ relationship of p-n junction with different doping profiles have been carried out. Also following the process discussed in section 3.2, the doping profiles in the highly doped p region have been extracted and compared with the originally defined doping profile.

3.3.1 p^+-n junction with uniformly doped n region

For a p^+-n junction shown in Figure 3.2, the n region is uniformly doped at a level of $1{\cdot}10^{18}$ cm^{-3}, the p region is Gaussian doped with a dose of $1{\cdot}10^{14}$ cm^{-2}, and with the characteristic length (standard deviation) of 3.5 nm, the depth of p region is approximately 10 nm. With depletion approximation, assuming the area of the p^+-n junction is 1 cm^2, following the process described in section 3.1, the $C(V_R)$ and $1/C(V_R)^2$ relationships are calculated and shown in Figure 3.3. It is shown that the $1/C^2$-V_R plots are linear, according to equation (2.31), the linearity indicates a uniform doping profile of the low doped n region.

删除的内容: (2.31)

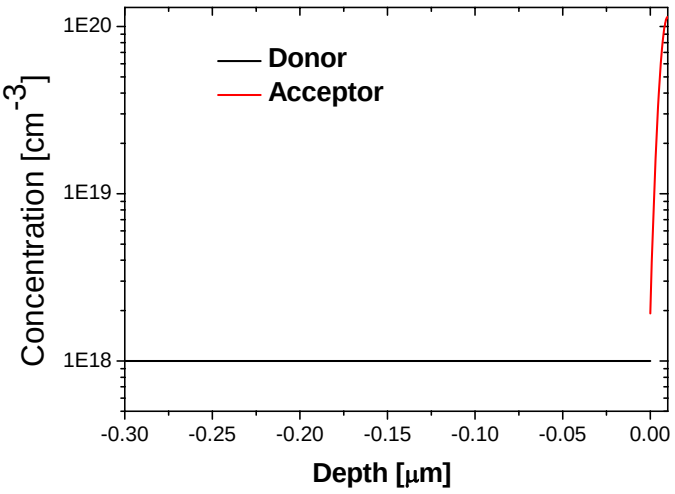

Figure 3.2 Doping profile of p^+-n junction with uniformly doped n region.

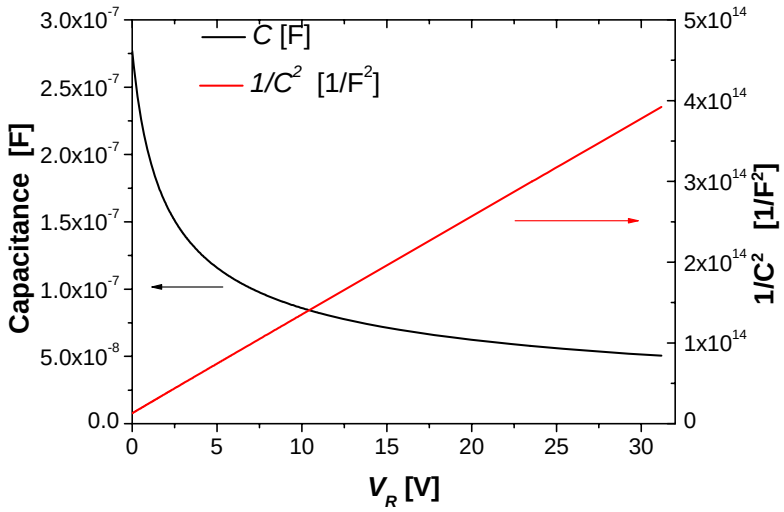

Figure 3.3 Analytically calculated $C(V_R)$ and $1/C(V_R)^2$ relationships of the p^+-n junction with a doping profile shown in Figure 3.3. During calculation the area of the diode is set to be 1 cm^2.

Based on the computed $C(V_R)$ relationship, following the process discussed in section 3.2, the doping profile in the highly doped p region has been computed with different assumptions of x_{n0}.The relationship between the assumed value of x_{n0} and the real value of x_{n0} can be expressed as

$$x_{n0\_assume} = x_{n0\_real} + \delta x_{n0} \tag{3.1}$$

In the equation above, x_{n0_assume} represents the assumed value of x_{n0}, x_{n0_real} is the original value of x_{n0} known from the calculation process of $C(V_R)$, and δx_{n0} is the difference between assumed value and true value of x_{n0}.

Figure 3.4 shows the estimated doping profile in the p region with different assumptions of x_{n0}. It is evident that if $x_{n0\_assume} = x_{n0\_real}$, the estimated doping profile in the p region fits perfectly with the defined doping profile. What is more, it is found that the error of x_{n0_assume} results in the same error of the position of the doping profile. However, as shown in Figure 3.4, the estimated doping concentration corresponding to different V_R does not depends on the assumption of x_{n0}. The phenomenon can be explained by the following discussion.

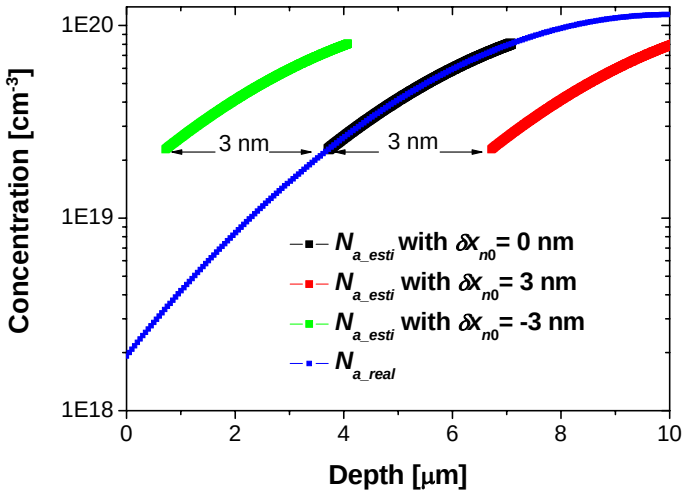

Figure 3.4 Estimated doping profile in the p region with different assumption of x_{n0}.

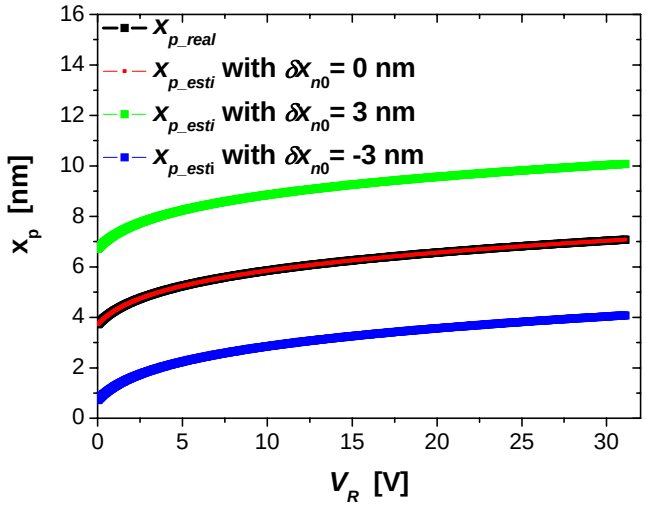

Figure 3.5 Estimated and real $x_p(V_R)$ relationship with different assumption of x_{n0}.

From equation (2.29), if $N_d(x)$ is constant throughout the n region, then at any bias

$$x_{n\_esti}(V_R) - x_{n0\_assume} = x_{n\_real}(V_R) - x_{n0\_real} \tag{3.2}$$

Combining equations (3.1) and (3.2), the following equation is given

删除的内容: (2.29)

删除的内容: (3.1)

删除的内容: (3.2)

$$x_{n\_esti}(V_R) = x_{n\_real}(V_R) + (x_{n0\_assume} - x_{n0\_real}) = x_{n\_real}(V_R) + \delta x_{n0} \quad (3.3)$$

Combining equation (2.17) and equation (3.3), it is found that

$$x_{p\_esti}(V_R) = x_{p\_real}(V_R) + \delta x_{n0} \quad (3.4)$$

The equation (3.4) can explain the phenomenon in Figure 3.6, that the estimated x_p at any bias has the same error as x_{n0_assume}.

When the calculation of the doping concentration is concerned, as shown in equation (2.29), for a certain $C(V_R)$ relationship, $W(V_R)$ and dW/dV_R can be calculated and are not dependent on the assumption of x_{n0}. Secondly N_d is constant through the n region and does not depend on x_{n0_assume} either. So with different x_{n0_assume}, the calculated values of N_a are the same with different assumptions of x_{n0} as shown in Figure 3.4.

Therefore, for p^+-n junction with uniform substrate, with different assumptions of x_{n0}, the estimated profiles are parallel to each other as indicated in Figure 3.4, and the abruptness of the doping profile in the highly doped p region can be accurately extracted.

3.3.2 p^+-n junction with step-like doped n region

For a p^+-n junction with stepped doping in the n region as shown in Figure 3.6, both the $C(V_R)$ and $1/C(V_R)^2$ relationships have been analytically computed and shown in Figure 3.7. As shown in Figure 3.6, L_{N1} is defined as the coordinate of the position where the doping profile in the n region increases abruptly.

删除的内容: (2.17)

删除的内容: (3.3)

删除的内容: (3.4)

删除的内容: (2.29)

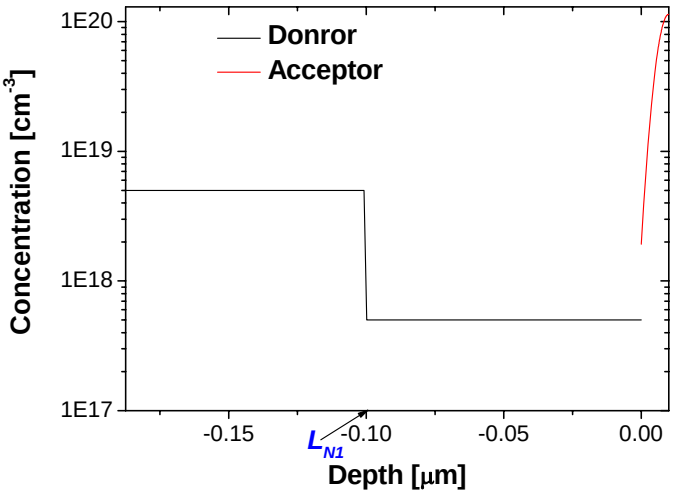

Figure 3.6 Doping profile of an ultra-shallow p^+-n junction with step-like doped n region.

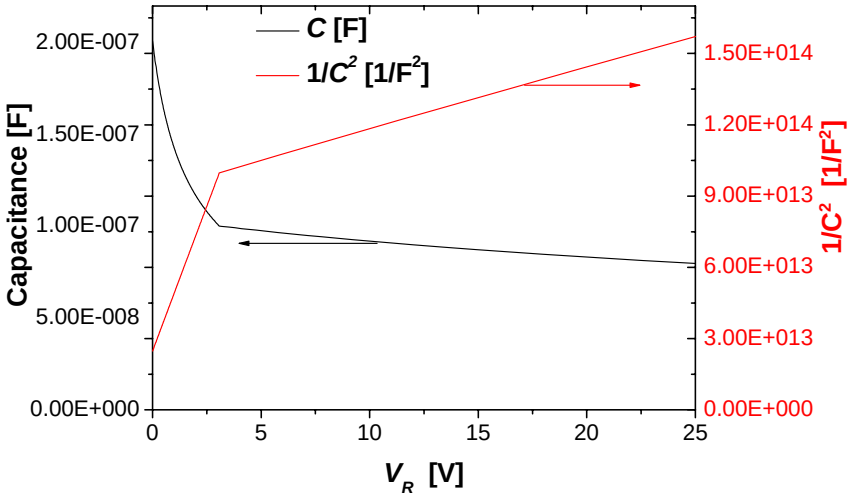

Figure 3.7 Analytically calculated $C(V_R)$ and $1/C(V_R)^2$ relationship of p^+-n junction with doping profile shown in Figure 3.6.

As shown in Figure 3.7, the $1/C^2$-V_R curve has two obviously different linear slopes which indicate that the low doped n region is step-like doped at two different concentrations (Fig. 3.6).

Based on the computed $C(V_R)$ relationship shown in Figure 3.7 and the doping profiles in the n region as shown in Figure 3.6, the profile in the p region has also been calculated with different assumptions of x_{n0}. With the correct assumption of x_{n0}, the doping profile in the highly doped p region accurately corresponds to the originally assumed doping profile, which is shown in Figure 3.8.

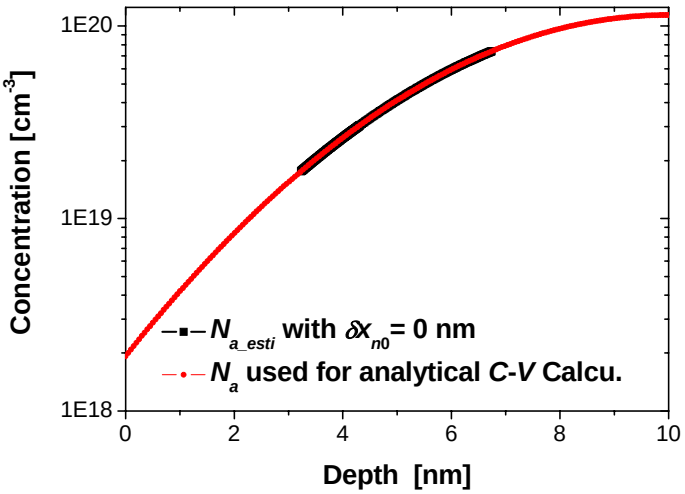

Figure 3.8 Estimated doping profile based on the $C(V_R)$ relationship shown in Figure 3.7 with the correct assumption of x_{n0}.

For a p^+-n junction with stepped profile in the n region, it is found that the assumption of x_{n0} will influence not only the estimated position coordinates of x_p but also the doping concentration. The estimated $x_p(V_R)$ relationship is shown in Figure 3.9: with an error of positive 3 nm, the value of estimated x_p decreases abruptly at some point. On the other hand, with an error of negative 3 nm, the value of estimated x_p increases abruptly at some point. This phenomenon can also be explained in the same way as discussed in section 3.3.1.

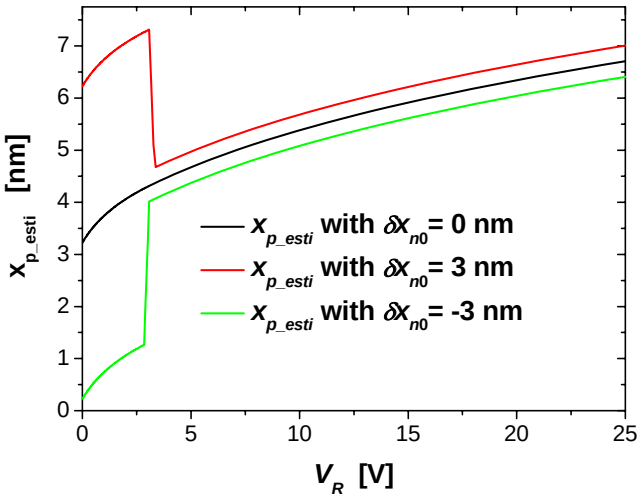

Figure 3.9 The estimated $x_p(V_R)$ relationship with different assumption of x_{n0}.

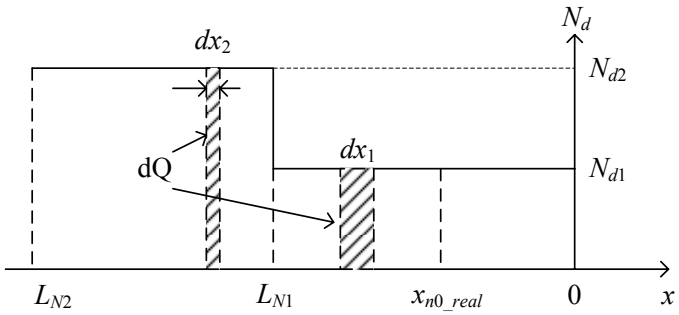

Figure 3.10 Schematic cross section of the doping profile in the stepped doped n region. To offer the same charge, different doping concentration results in different depletion width.

As indicated by equation (2.27), as V_R increases, the depletion region increases in the minus x direction as shown in Figure 3.1. As shown in Figure 3.10, for the same amount of charge, higher doped region requires narrower region to be depleted.

删除的内容: (2.27)

If the assumed x_{n0} is larger than the real x_{n0}, taking $\delta x_{n0} = 3$ nm for example, compared with $\delta x_{n0} = 0$ nm, the estimated x_n with $\delta x_{n0} = 3$ nm would reach L_{N1} later. With $\delta x_{n0} = 3$ nm, $V_{R1.1}$ and $V_{R1.2}$ are defined as the reverse biases at which the following two equations are satisfied.

$$x_{n\_esti}(V_{R1.1}) = L_{N1} + \delta x_{n0} \tag{3.5}$$

$$x_{n\_esti}(V_{R1.2}) = L_{N1} \tag{3.6}$$

The definitions of $V_{R1.1}$ and $V_{R1.2}$ with $\delta x_{n0} = 3$ nm are clearly shown in Figure 3.11. With $\delta x_{n0} = 3$ nm, before reaching $V_{R1.1}$, the step of calculated x_n is the same as that with $\delta x_{n0} = 0$ nm. However, after reaching $V_{R1.1}$, the real concentration in the depletion region becomes different from the expected concentration. As a consequence, the step of estimated x_n becomes much larger than the real step ought to be according to the C-V dependence, until reaching $V_{R1.2}$. As a result, the calculated x_p will decrease abruptly between $V_{R1.1}$ and $V_{R1.2}$ as indicated in Figure 3.9.

Analogously, if the assumed x_{n0} is smaller than the real x_{n0}, taking $\delta x_{n0} = -3$ nm for example, the estimated x_n would reach L_{N1} earlier compared with the case of $\delta x_{n0} = 0$. With $\delta x_{n0} = -3$ nm, $V_{R2.1}$ and $V_{R2.2}$ are defined by the following two equations respectively.

删除的内容: is defined by the following equation

$$x_{n\_esti}(V_{R2.1}) = L_{N1} \tag{3.7}$$

$$x_{n\_real}(V_{R2.2}) = L_{N1} \tag{3.8}$$

Also, the definitions of $V_{R2.1}$ and $V_{R2.2}$ with $\delta x_{n0} = -3$ nm are indicated in Figure 3.11. With $\delta x_{n0} = -3$ nm, before reaching $V_{R2.1}$, the step of calculated x_n is the same as that with $\delta x_{n0} = 0$ nm. But when the reverse bias is in the interval between $V_{R2.1}$ and $V_{R2.2}$, as a result of the concentration difference, the computed depleted width step in the n region is much smaller, so the estimated x_p will increase abruptly between $V_{R2.1}$ and $V_{R2.2}$ as shown in Figure 3.9.

This phenomenon demonstrates that it is possible to determine the real value of x_{n0} based on the $C(V_R)$ of p^+-n junction and known stepped doping profile in the n region. Assuming different values of x_{n0}, different $x_{p\_esti}(V_R)$ relationships can be calculated, and only with the correct assumption of x_{n0}, the computed x_p and the p doping profile will smoothly increase as V_R increases. So based on different evaluations of $x_{p\_esti}(V_R)$ with different assumptions of x_{n0}, the accurate value of x_{n0_real} can be extracted.

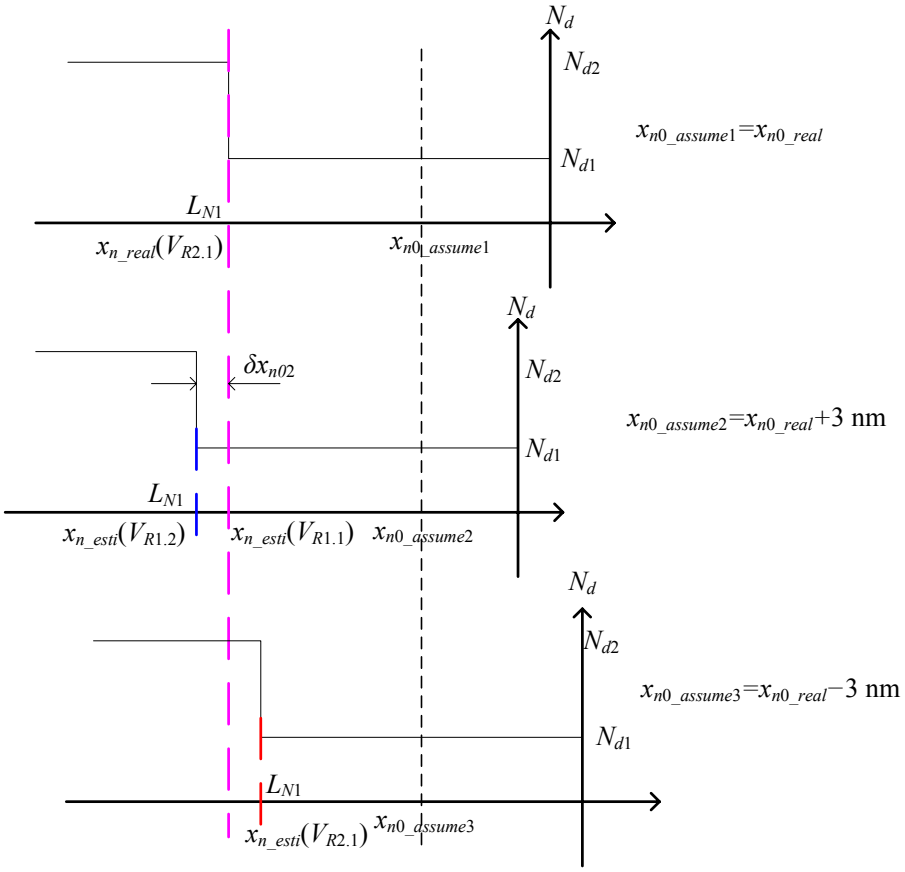

Figure 3.11 Definitions of $V_{R1.1}$ and $V_{R1.2}$ with $\delta x_{n0} = 3$ nm, and $V_{R12.1}$ and $V_{R2.2}$ with $\delta x_{n0} = -3$ nm.

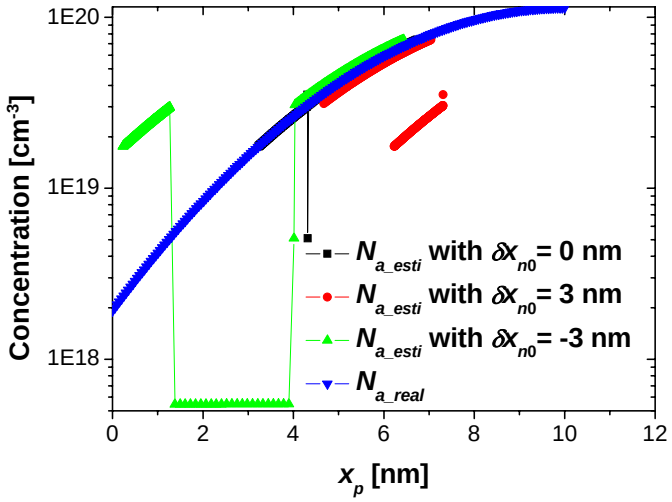

Figure 3.12 Estimated $N_a(x_p)$ with different assumptions of x_{n0}.

Regarding the estimation of the doping concentration, according to equation (2.29), since $N_d(x)$ is not uniform throughout the n region, the estimated $N_d(x_n)$ can be influenced by the assumption of x_{n0}. As a result, even though $W(V_R)$ and dW/dV_R do not depend on the assumption of x_{n0}, $N_{a\_esti}(x)$ does depend on the assumption of x_{n0} as shown in Figure 3.12.

删除的内容: (2.29)

From Figure 3.12, it is found that for p^+-n junction with step-like n profile, with an error of ±3 nm of the assumed value of x_{n0}, neither $x_p(V_R)$ nor N_a can be correctly calculated. However, it is also shown that, with the right assumption of x_{n0}, the computed doping profile in the p region fits perfectly with the defined doping profile.

删除的内容: assumed

In summary, for a p^+-n junction with a stepped doping profile in the n region, based on the analytically calculated $C(V_R)$ relationship, the accurate value of x_{n0_real} can be extracted by computing and comparing $x_{p\_esti}(V_R)$ and $N_{a\_esti}(x)$ relationships with different assumptions of x_{n0}. What is more, it is demonstrated that with right x_{n0}, the doping profile in p^+ region can be accurately calculated.

References

[1] Donald A.Neamen, Semiconductor Physics and Devices: Basic Principles, 3rd ed. New York, USA: McGraw-Hill, 2003.
[2] S.M.Sze, Semiconductor Devices: Physics and Technology, 2nd ed.

New York,USA : Wiley, 2002
[3] H. J. J. De Man. On the Calculation of Doping Profile from C (V) Measurement on Two-sided Junctions. IEEE Transactions on Electron Devices, 1970, December, Vol. 17:1087
[4] Walter C. Johnson, Peter T. Panousis, The influence of Debye Length on the *C-V* Measurement of Doping Profiles. IEEE Transaction Devices, 1971, October, NO.10, vol. ED-18:965

Chapter 4 Two-sided *C-V* profiling based on Medici simulations

As discussed in Chapter 3, for a p^+-n junction with stepped n doping profile, x_{n0} and p doping profile can be accurately computed based on the knowledge of the n doping profile and the analytically calculated $C(V_R)$ relationship under depletion approximation. However in depletion approximation [1], it is assumed that the semiconductor is divided into two distinct kinds of regions, one is fully depleted of charge carriers, the other is absolutely charge neutral. Debye screen length is assumed to be zero. Experimentally, the diffusion and transport of carriers cannot be neglected. What is more, the doping profile in the n region cannot be taken as known directly.

In this chapter, we prove the validity of the two-sided profiling technique by applying the profiling method based on $C(V_R)$ relationship of p^+-n diode obtained using a 1-D Medici device simulation instead of the analytical calculation. In Medici simulations, unlike in analytical calculations, firstly, the diffusion of electrons and holes is considered, so the electron and hole profiles are a bit different from the doping profile. Secondly, the abrupt depletion approximation is discarded.

In this chapter, a p^+-n junction and an n-Schottky diode with the same n doping profiles as that of p^+-n are designed. First of all, Medici simulations are carried out for the $C(V_R)$ relationship of p^+-n and n-Schottky diodes. Secondly, using the conventional *C-V* profiling of the n-Schottky diode, the electron profile of Schottky diode at thermal equilibrium is obtained and taken as n doping profile of both the Schottky diode and the p^+-n diode. Then, based on the $C(V_R)$ relationship of p^+-n diode and calculated n profile, the two-sided *C-V* profiling technique discussed in Chapter 3 is applied to predict the doping profile in the p region. It is confirmed that, if the doping profile in the n region is uniform, the abruptness of p doping profile can be accurately extracted. On the other hand, if the doping profile in the n region is step-like, both x_{n0} and p^+ doping profiles can be exactly estimated.

4.1 Profiling with a uniform n profile

In this section, the two-sided profiling technique presented in Chapter 2 is implemented based on the Medici simulated $C(V_R)$ relationship of p^+-n and Schottky diodes with the same uniformly doped n region. The schematic cross sections of the 1-D Medici simulated p^+-n and Schottky diodes are shown in Figure 4.1. At thermal

equilibrium, the defined doping profile and Medici simulated carrier profiles of the p^+-n junction with uniformly doped n region are shown in Figure 4.2. The Schottky diode has the same n doping profile as the p^+-n junction. The areas of the p^+-n diode and Schottky diode are both set to be 1 μm × 1 μm.

During 1-D Medici device simulations [3], DC solutions of Schottky and p^+-n diode are solved at different reverse bias voltages, 0-25V and 0-15V with a step of 0.1V respectively. The larger bias range of the n-Schottky diode is to make sure that the calculated n profile is deep enough for the two-sided profiling of the p^+-n diode. In practice, the Schottky diode will have a smaller breakdown voltage and a higher leakage current, so this will not be possible. During this process, the Poisson's equation, continuity equations and the Boltzmann equation are all coupled and solved numerically. Medici performs AC analysis as a post-processing step after reaching a DC solution [3]. AC small signal simulations are carried out at each DC bias by applying a sinusoidal signal at a frequency of 1 MHz with an amplitude of 10 mV. The simulated C-V_R and $1/C^2$-V_R curves of p^+-n and Schottky diodes are shown in Figure 4.3. According to equations (2.31) and (2.40), the uniformity of the doping profile in the n region accounts for the linearity of $1/C^2$-V_R curves.

删除的内容: (2.31)

删除的内容: (2.40)

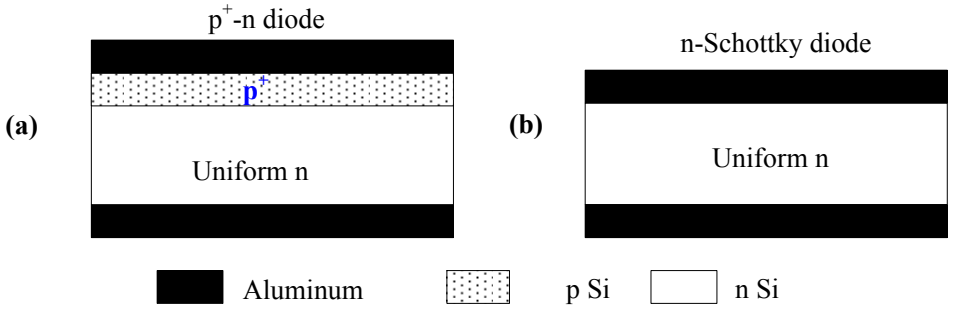

Figure 4.1 (a) Schematic cross section of the p^+-n diode with uniformly doped n region (b) n-Schottky diode with the same uniformly doped n region as the p^+-n diode.

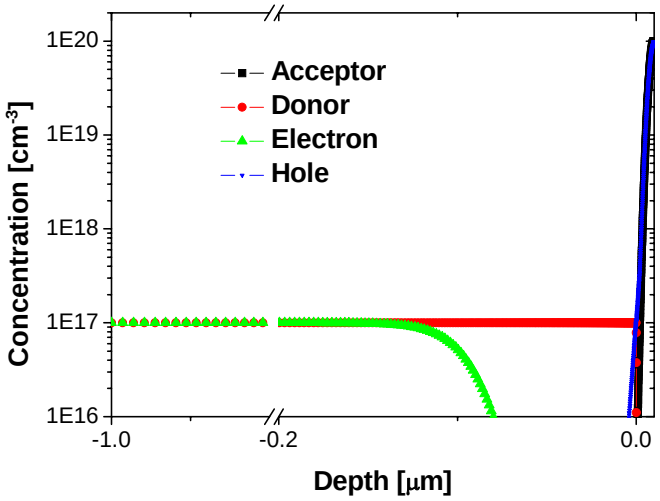

Figure 4.2 Doping profiles of the simulated p^+-n junction and the simulated carriers distribution at thermal equilibrium.

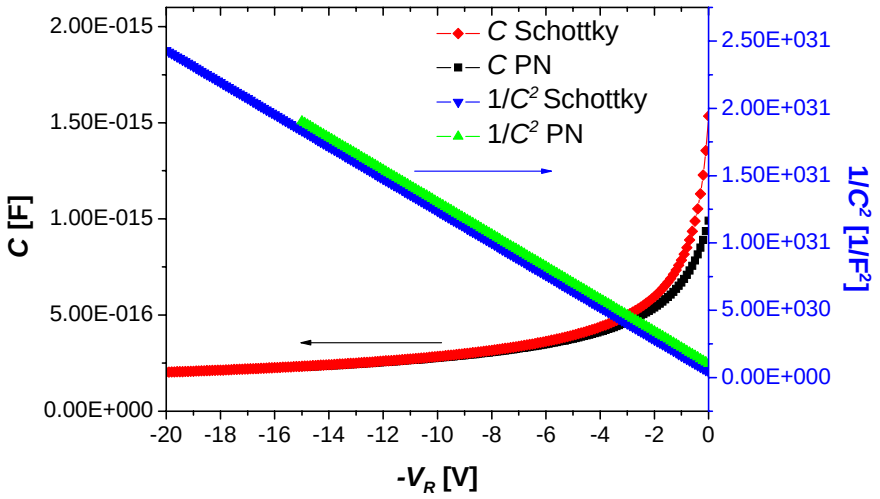

Figure 4.3 Simulation of $C(V_R)$ and calculation of $1/C^2(V_R)$ relationship of p-n and Schottky diodes.

Firstly, based on the simulated C-V_R data of the n-Schottky diode, the doping profile in the n region is estimated and shown in Figure 4.4. It is clearly shown that, the estimated doping profile fits very well with the doping profile used in the simulation. Secondly, based on the simulated C-V_R data of the p^+-n diode, the $W(V_R)$ relationship

of the p^+-n diode is computed. Thirdly, using equation (2.27), taking the estimated doping profile of the n-Schottky diode as the n profile of the p^+-n diode, the $x_n(V_R)$ relationship is calculated with different assumption of x_{n0} and denoted as $x_{n\_esti}(V_R)$. After that, using equation (2.28), the $x_p(V_R)$ relationships are computed with different assumption of x_{n0}, identified as $x_{p\_esti}(V_R)$ and shown in Figure 4.5. In the end, using equation (2.29), the doping profile in the highly doped region is computed with different assumption of x_{n0}.

删除的内容: (2.27)

删除的内容: (2.28)

删除的内容: (2.29)

As shown in Figure 4.5, with three different assumption of x_{n0}, the three different $x_{p\_esti}(V_R)$ curves are in parallel with each other. As labeled in the figure, the difference between two different $x_{p\_esti}(V_R)$, is exactly equal to the difference of the assumed x_{n0}. This regularity is in accordance with that of two sided profiling based on the analytically calculated $C(V_R)$ relationship of p^+-n junction with a uniformly doped n region.

The estimated p^+ doping profiles with different assumptions of x_{n0} are shown in Figure 4.6: it is found that when $x_{n0} = -100.7$ nm, the estimated doping profile fits well with the simulated hole profile at thermal equilibrium. With three different assumption of x_{n0}, the three $x_{p\_esti}(V_R)$ curves are in parallel with each other. So even with a wrong assumption of x_{n0}, the doping gradient in the highly doped p region can be exactly estimated.

As shown in Figure 4.4, the starting depth of the depletion region of the Schottky diode is smaller than 100.7 nm, which indicates that at thermal equilibrium, the edge of the n depletion region of the Schottky diode is shallower than the edge of the n depletion region of the p^+-n diode. This will practically always be the case due to both diffusion of acceptors and holes into the n region and the fact that the potential drop over a p-n junction is larger than that of the Schottky junction.

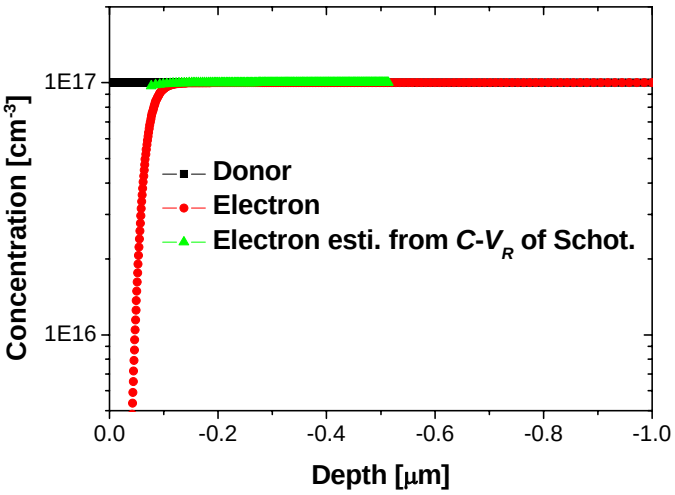

Figure 4.4 Estimated electron (donor) profile in the n region of Schottky diode, the defined doping profile and Medici simulated electron profile at thermal equilibrium.

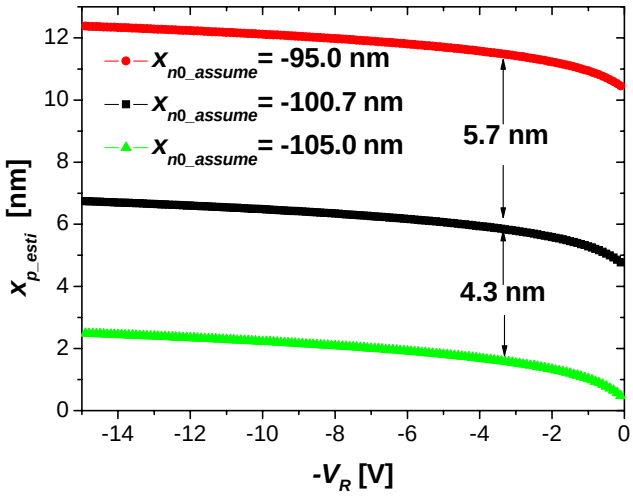

Figure 4.5 With different assumptions of x_{n0}, estimated boundaries of depletion region to the neutral p region at different applying biases.

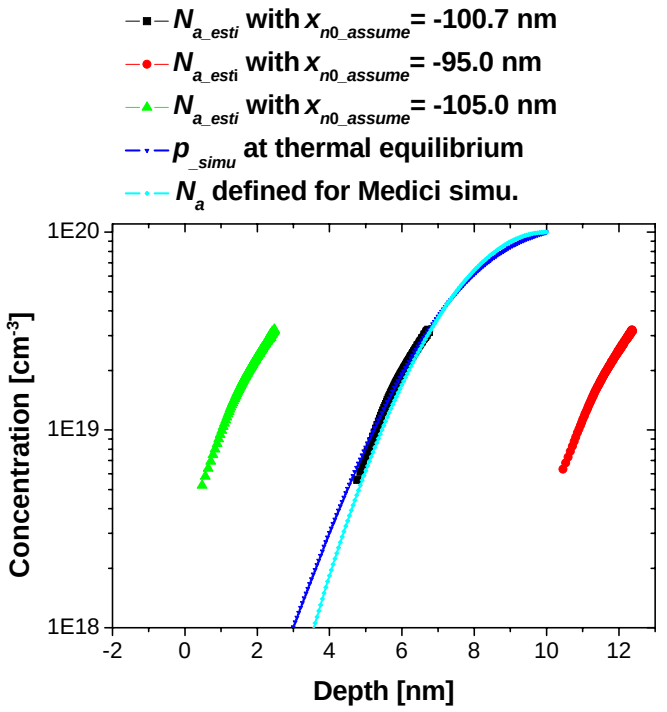

Figure 4.6 Estimation of doping profile in the p^+ region with different assumptions of x_{n0}, compared with the defined acceptor profile for Medici simulation and the Medici simulated hole profile at thermal equilibrium,

4.2 Profiling with a step-like n profile

Also, the two-sided profiling method discussed in Chapter 3 is applied for the profiling of the doping profile in the highly doped p region of p^+-n junction with step-like n profile. The 1-D simulation structures of p^+-n and n-Schottky diode are shown in Figure 4.7. The n-Schottky diode has the same step-like n profile as p^+-n junction.

Medici simulations [3] are implemented for p^+-n and Schottky diodes with the same step-like doping profile in the n region. At thermal equilibrium, the defined doping profile and Medici simulated carrier profiles of p^+-n junction with a stepped n profile are shown in Figure 4.8. The areas of the p^+-n diode and Schottky diode are both set to 1 µm × 1 µm. During Medici simulations, with a step of 0.1 V, the reverse applied voltage changes from 0 V to 25 V and 15 V for Schottky and p^+-n junctions respectively, DC solutions at each bias are obtained by solving the coupled Poisson's

equation, continuity equations and the Boltzmann Equation together.

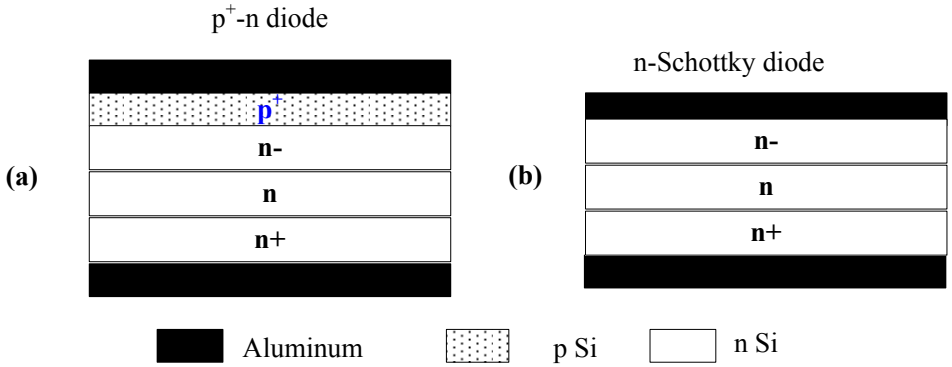

Figure 4.7 (a) Schematic cross section of the p^+-n diode with stepped n doping profile (b) n-Schottky diode with the same stepped n doping profile as the p^+-n diode.

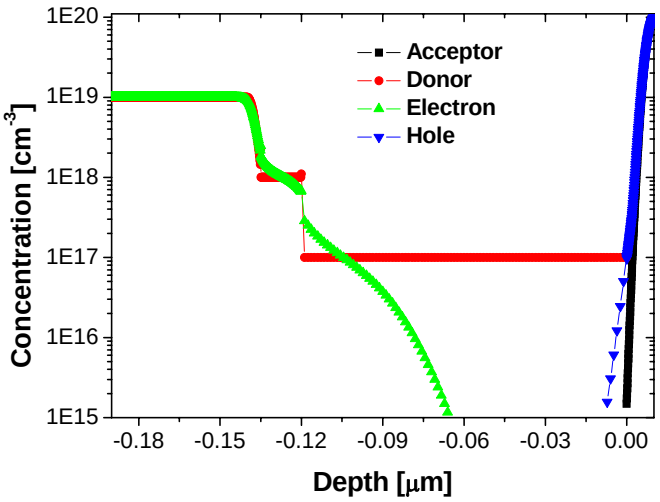

Figure 4.8 Simulations of doping and carrier density profiles of p^+-n junction at thermal equilibrium.

The capacitance versus applied voltage relationship is computed by applying a small sinusoidal signal with an amplitude of 10 mV, at a frequency of 1 MHz. The simulated $C(V_R)$ characteristics of p^+-n diode with doping profiles shown in Figure 4.8 and Schottky diode with same n doping profile are shown in Figure 4.9. What is more, $1/C(V_R)^2$ curves of p^+-n and Schottky diodes are calculated and shown in Figure 4.9. Unlike the analytically calculated $1/C(V_R)^2$ curve of the p^+-n diode with step-like n profile, the $1/C(V_R)^2$ curves of p^+-n and Schottky diodes are not exactly piecewise

linear.

This phenomenon can be explained by the simulated electron profile of p^+-n and Schottky diode at thermal equilibrium. As shown in Figure 4.8 and Figure 4.10, as a result of the diffusion, the electron profiles of both the p^+-n diode and the Schottky diode at thermal equilibrium are not exactly step-like as the doping profile.

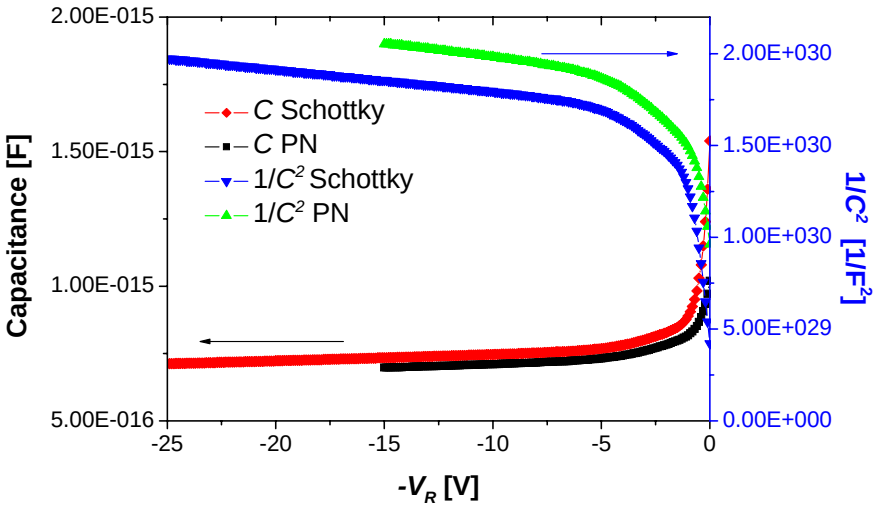

Figure 4.9 Simulation of the $C(V_R)$ and calculation of the $1/C(V_R)^2$ relationships of p^+-n diode and n-Schottky diode with the same stepped n doping profile.

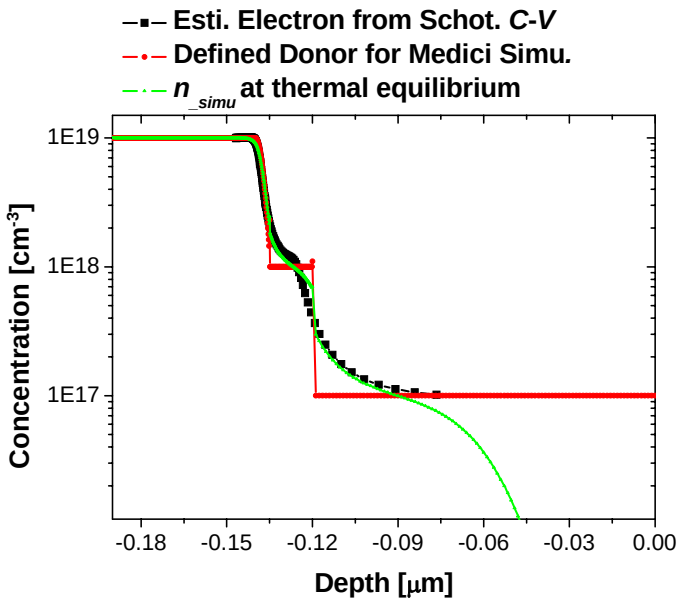

Figure 4.10 Simulation of the electron profile at thermal equilibrium and *C-V* profiling of the n profile of the n-Schottky diode.

Then based on the *C-V* data of Schottky diode, using equation (2.40), the doping profile in the n region is calculated and shown in Figure 4.10, also the defined doping profile and Medici simulated electron profile at thermal equilibrium are shown in the same figure. It is found that the computed doping profile fits quite well with the original electron profile. A small discrepancy between the simulated electron profile and the profile obtained from the *C-V* characteristic originates from the fact that in the calculation of the profile a depletion approximation is made, unlike in the simulation of the *C-V* curve.

删除的内容: (2.40)

Taking the estimated donor profile the of Schottky diode as the donor profile of the p^+-n diode, based on the simulated *C-V* relationship of p^+-n junction, two-sided profiling method is implemented with different assumptions of x_{n0}. In this process, different $x_{p\_esti}(V_R)$ relationships are calculated with different assumptions of x_{n0} and shown in Figure 4.11.

As shown in Figure 4.11, based on the Medici simulated *C-V* data of p^+-n and Schottky diodes with stepped n doping profile, with larger x_{n0_assume}, the estimated $x_p(V_R)$ relationships decrease at the first few bias points. This can be explained by the following discussion. As indicated in Figure 4.10, as x_{n0_assume} increases, the estimated electron profile decreases. As a result, for the same amount of electrons to be depleted,

if x_{n0_assume} is lager than the real value of x_{n0}, the step width of $x_{n\_esti}(V_R)$ will be larger than the real values. If the assumed x_{n0} is too large, the step width of estimated $x_{n\_esti}(V_R)$ can be even larger than the step of $W(V_R)$, which induces $x_{p\_esti}(V_R)$ to decrease at the first few points. This phenomenon is shown in details in Figure 4.12, with x_{n0_assume} equals –96.0 nm, at the first few bias points, the step width of $x_{n\_esti}(V_R)$ is larger than that of $W(V_R)$, and as a result, the step of $x_{p\_esti}(V_R)$ is negative and $x_{p\_esti}(V_R)$ decreases at the first few bias points which is in accordance with Figure 4.11. This phenomenon offers one way to determine the upper limit of x_{n0}. In this case, the limit is that the assumed x_{n0} should be smaller than − 97.3 nm as indicated in Figure 4.11.

We will now consider what will happen if the assumed x_{n0} is too small. Wrong x_{n0_assume} would results in both wrong x_{p_esti} and N_{a_esti}. But if x_{n0_assume} is smaller than x_{n0_real}, taking $x_{n0\_assume} = -99.0$ nm for example, $x_{p\_esti}(V_R)$ plot would not be obviously anomalous and it is impossible to judge whether x_{n0_assume} is too small or not from the $x_{p\_esti}(V_R)$ plot, as shown in Figure 4.11. But the estimated doping profile is abnormal judging from the phenomenon that the slope of the estimated p^+ doping profile is not smooth, as shown in Figure 4.13. This phenomenon can be used for the extraction of the lower limit of x_{n0}. Firstly, based on the knowledge $C(V_R)$ relationship and the n doping profile of p^+-n diode, with different x_{n0_assume}, calculated the $x_{p\_esti}(V_R)$ and $N_{a\_esti}(x)$ relationship. Secondly, the critical value of x_{n0_assume} where $x_{p\_esti}(V_R)$ changes from abnormal to normal can be set as the upper limit of x_{n0} which is specified as x_{n0_max}. Thirdly, analyze the $N_{a\_esti}(x)$ relationship with x_{n0_assume} smaller than x_{n0_max}, the critical value of x_{n0_assume} where $N_{a\_esti}(x)$ starts exhibiting unexpected features such as non-monotonicity or concaveness can be set as the lower limit of x_{n0} which is specified as x_{n0_min}. It is not possible to obtain a single x_{n0_assume} value that would be exactly equal to x_{n0_real}, however, assuming one value of x_{n0_assume} between x_{n0_min} and x_{n0_max}, $x_{p\_esti}(V_R)$ and $N_{a\_esti}(\mathrm{x})$ should be very close to the true values as the interval (x_{n0_min}, x_{n0_max}) is according to the results simulated here around 1 nm wide.

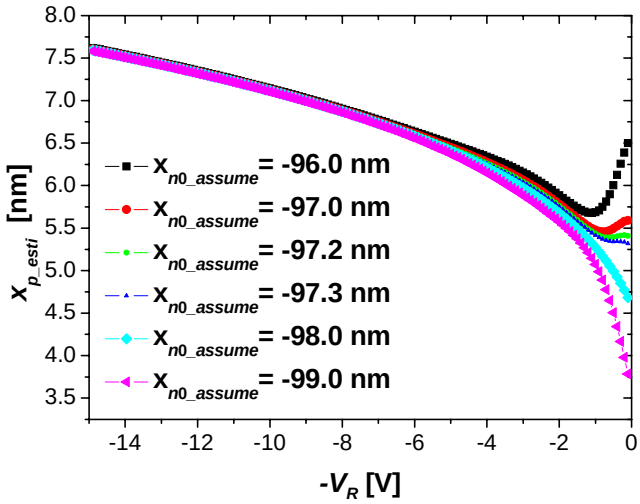

Figure 4.11 Estimated x_p versus reverse applied voltage with different x_{n0} supposed.

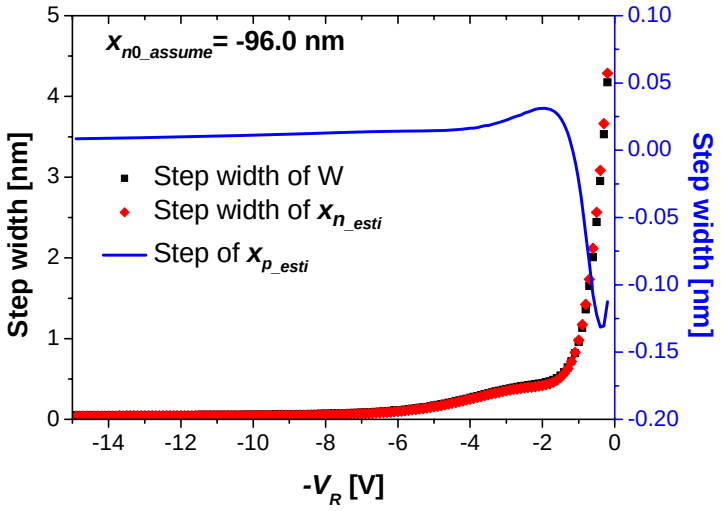

Figure 4.12 With $x_{n0\_assume} = -96.0$ nm, steps of depletion width, estimated x_n and x_p as function of reverse applied voltage.

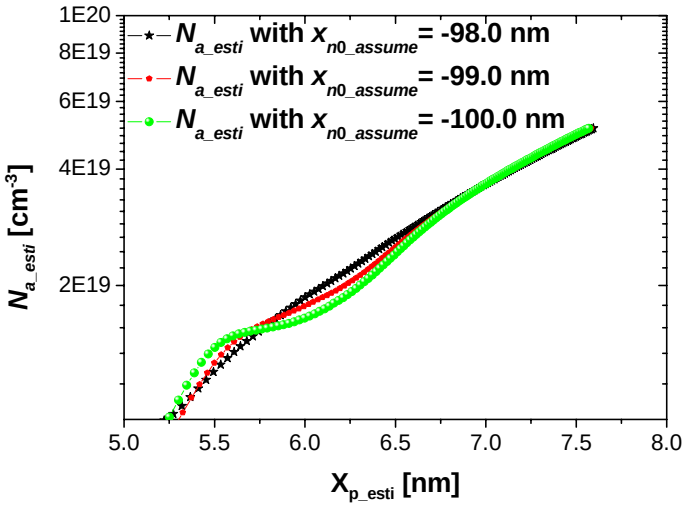

Figure 4.13 Estimated p^+ doping profile with x_{n0_assume} = −98.0 nm, −99.0 nm and −100.0 nm.

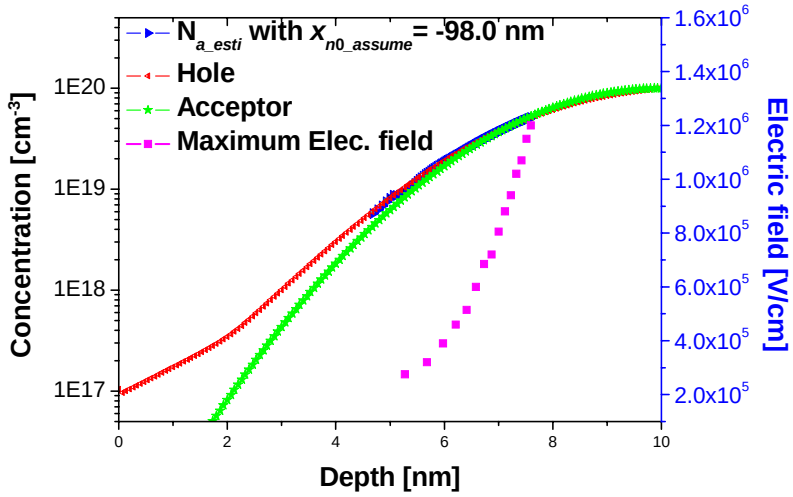

Figure 4.14 Acceptor profile estimated with x_{n0_assume} = −98.0 nm, and the simulated acceptor profile and hole profile at thermal equilibrium.

As the profiling of the Medici simulated p^+-n junction is concerned, x_{n0_min} and x_{n0_max} are −99.0 nm and −97.0 nm respectively. With x_{n0_assume} = −98.0 nm, the estimated doping profile in the highly doped region fits well with the hole density distribution at thermal equilibrium and shown in Figure 4.14. Also, the maximum electric field of

the junction versus the estimated x_p relationship is shown in Figure 4.14, as the depletion region width increases, the maximum electric field of the junction also increases.

We can come to the conclusion that for p^+-n and n-Schottky diodes with the same step-like n profile, using two-sided profiling technique, the value of both x_{n0_real} and the doping profiles in the p^+ region can be exactly computed.

4.3 Experiments and measurements

According to the two-sided C-V profiling based on Medici simulations, for p^+-n and n-Schottky diodes with the same step-like n profile, using two-sided profiling technique, both x_{n0} and the doping profiles in the p^+ region can be exactly computed. So, test structures of p^+-n and n-Schottky diodes with the same step-like n profile have been fabricated and measured. Two groups of samples have been fabricated. The Schematic cross section of sample A is shown in Figure 4.15. The different layers with different doping profile are grown layer by layer using epitaxy. For comparison, sample B is fabricated with 10 minutes thermal annealing after the fabrication of sample A.

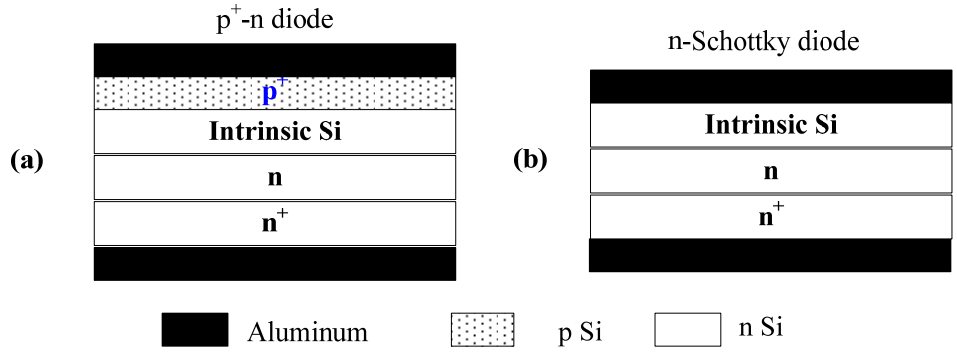

Figure 4.15 Schematic cross section of sample A: p+-n and n-Schottky diode with the same stepped n doping profile.

Based on the measured C-V_R relationship of p-n and Schottky diodes, two-sided C-V profiling has been carried out for the doping profile in the highly doped p region. The extracted p doping profiles of samples A and B are shown in Figure 4.16. As indicated in Figure 4.16, the junction depth of B sample is larger than that of A sample, and the doping gradient of B sample is smaller than that of A sample. This is in accordance with the fact that the 10 minutes thermal annealing will induce the diffusion of acceptors from the highly doped p region to the n region.

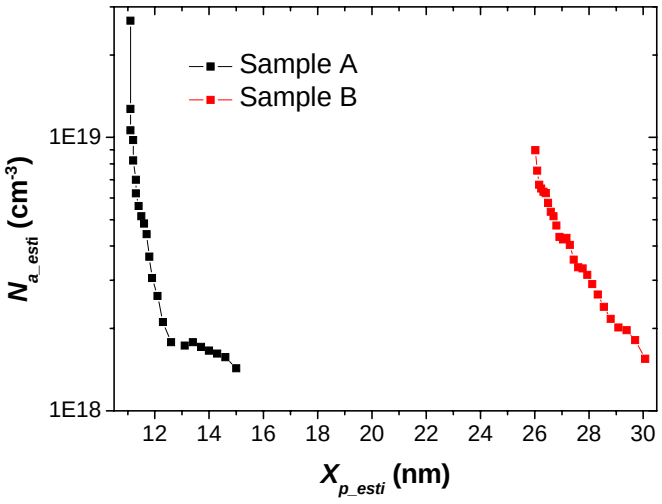

Figure 4.16 Extracted doping profile of the ultra-shallow p^+ region.

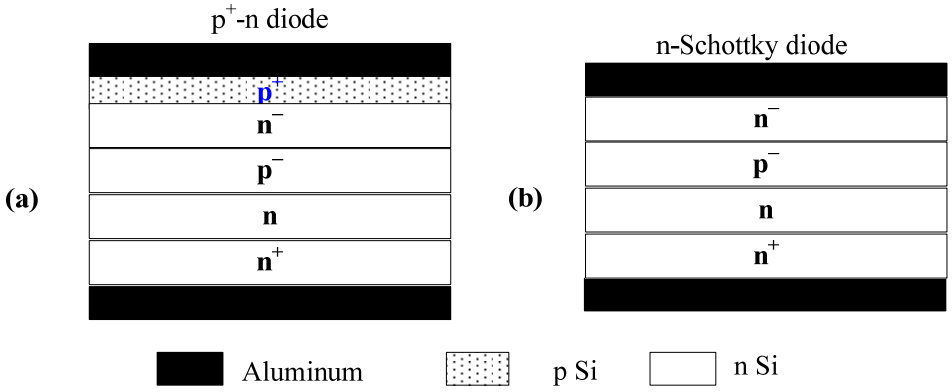

Figure 4.17 Recommended test structures to improve the breakdown voltage.

From the measurement of C-V_R relationships of the p^+-n^--n-n^+ and Schottky- n^--n-n^+, it is found that the breakdown voltage is around 4 V for p-n diode and 3 V for Schottky diode. The low breakdown voltages have limited the application of the two-sided C-V profiling, and only a small part of the doping profile can be estimated. The test structure shown in Figure 4.17 is recommended to improve the breakdown voltage. With optimized design, the n^- and p^- region can be fully depleted at thermal equilibrium, thus the depletion region width and breakdown voltage will increase compared with the fabricated test structure. What is more, the leakage current of the fabricated test structure is shown to be too large, in the future work, we can try to improve the fabrication process and do C-V measurement at a higher frequency.

删除的内容: p^+-n^--p^--n-n^+ and Schottky- n^--p^--n-n^+

References

[1] Walter C. Johnson, Peter T. Panousis, The influence of Debye Length on the *C-V* Measurement of Doping Profiles. IEEE Transaction Devices, 1971, October, NO.10, vol. ED-18:965
[2] H. J. J. De Man. On the Calculation of Doping Profile from C (V) Measurement on Two-sided Junctions. IEEE Transactions on Electron Devices, 1970, December, Vol. 17:1087
[3]http://www.synopsys.com

5 Extraction of minority carrier lifetime and surface recombination velocity of Al-doped SPE ultra-shallow p^+-n junctions

At DIMES a solid phase epitaxy (SPE) process has been developed based on material inversion of amorphous silicon on an aluminum layer-stack [1, 2, 3]. This technology is excellent for ultra-shallow junction fabrication, as it can provide a defect-free interface, low-ohmic contact resistance and an abrupt junction without diffusion. Based on this technology, p^+-p^- and p^+-p^+ contacts, p^+-n diodes and p^+-n-p bipolar transistors with near ideal electrical characteristics have been fabricated.

Minority carrier lifetime τ and surface recombination velocity v are necessary parameters for device modeling. In this chapter are presented the results of how τ and v are extracted following two steps: (1) Extracting the area current density of the collector current I_C and the base current I_B based on the Gummel characteristics of the fabricated p^+-n-p BJTs with different sizes of Al-doped SPE emitters. (2) Carrying out 1-D Tsuprem4 and Medici simulations for the area current densities of I_C and I_B, modulating τ and v to achieve good fitting between the simulated area current densities and the extracted area current densities.

5.1 Extraction of the area current component density of collector and base current

The total current of a diode is composed of the area, perimeter and corner current contributions. In this section, according to the geometry scaling rule of the junction current, the area current density of I_C and I_B are extracted.

5.1.1 Derivation of the formulas for the extraction of the area current component

If we consider the current at certain biasing voltages, the total current of a junction can be described as a sum of the area, perimeter and corner components by the

following equation [4]

$$I = I_A \times A + I_P \times P + I_K \tag{5.1}$$

I_A is the area current density, A is the area of junction, I_P is the perimeter current density, P is the perimeter of junction, I_K represents the corner current.[3]

For square devices with side length L, we have

$$A = L^2 \tag{5.2}$$
$$P = 4 \times L \tag{5.3}$$

Combining equations (5.1), (5.2), (5.3), yields

$$I = I_A \times L^2 + 4I_P \times L + I_K \tag{5.4}$$

For two devices with the same doping profile and different side lengths L_1 and L_2,

$$I_1 = I_A L_1^2 + 4I_P L_1 + I_K \tag{5.5}$$

$$I_2 = I_A L_2^2 + 4I_P L_2 + I_K \tag{5.6}$$

Subtracting equation (5.5) from the equation (5.6) we get

删除的内容: (5.5)

删除的内容: (5.6)

$$\frac{I_2 - I_1}{L_2 - L_1} = I_A(L_2 + L_1) + 4I_P \tag{5.7}$$

The real side length of the contact L can, and generally speaking does deviate from the nominal length (mask length) L_m. We assume that the deviation is approximately constant regardless of the contact size, so that

$$L_1 = L_{m1} + \Delta L \tag{5.8}$$

$$L_2 = L_{m2} + \Delta L \tag{5.9}$$

Combining equations (5.8) and (5.9), it is found

删除的内容: (5.8)

删除的内容: (5.9)

$$L_2 - L_1 = L_{m2} - L_{m1} \tag{5.10}$$

$$L_2 + L_1 = L_{m2} + L_{m1} + 2\Delta L \tag{5.11}$$

Substituting equations (5.10) and (5.11) into equation (5.7), we obtain

删除的内容: (5.10)

删除的内容: (5.11)

删除的内容: (5.7)

$$\frac{I_2 - I_1}{L_{m2} - L_{m1}} = I_A(L_{m2} + L_{m1}) + 2I_A \times \Delta L + 4I_P \tag{5.12}$$

For a series of devices with different L_m, the values of $(I_2\text{-}I_1)/(L_{m2}\text{-}L_{m1})$ and $(L_{m2}+L_{m1})$ of each couple of devices with different L_m can be calculated. Then from the linear fitting between $(I_2\text{-}I_1)/(L_{m2}\text{-}L_{m1})$ and $(L_{m2}+L_{m1})$, the slope I_A which stands for the area current density can be extracted.

5.1.2 Extraction of the area current density of I_C and I_B

Measurements were performed on p^+-n-p BJTs with Al-doped SPE emitters which were successfully fabricated and shown to have near-ideal electrical characteristics. Six of the fabricated p^+-n-p BJTs with square emitters with different L_m (0.8 μm, 0.9 μm, 1 μm, 1.2 μm, 1.4 μm, and 1.6 μm) are chosen for the extraction of the area current density of I_C and I_B.

Based on the measured near ideal Gummel plots of the six p^+-n-p BJTs, for both I_C and I_B, the values of $(I_2-I_1)/(L_{m2}-L_{m1})$ and $(L_{m2}+L_{m1})$ of each couple of devices with different L_m are calculated respectively. Then, according to equation (5.12), from the linear fitting between $(I_2-I_1)/(L_{m2}-L_{m1})$ and $(L_{m2}+L_{m1})$, the area current density of both I_C and I_B under different bias conditions are extracted and shown in Table 5.1. When $V_{CB}=0$, $V_{EB}=0.7$ V, the linear fitting between $(I_2-I_1)/(L_{m2}-L_{m1})$ and $(L_{m2}+L_{m1})$ for both I_C and I_B is shown in Figure 5.1, the slopes I_{CA} and I_{BA} stand for the area current density of I_C and I_B respectively.

删除的内容: (5.12)

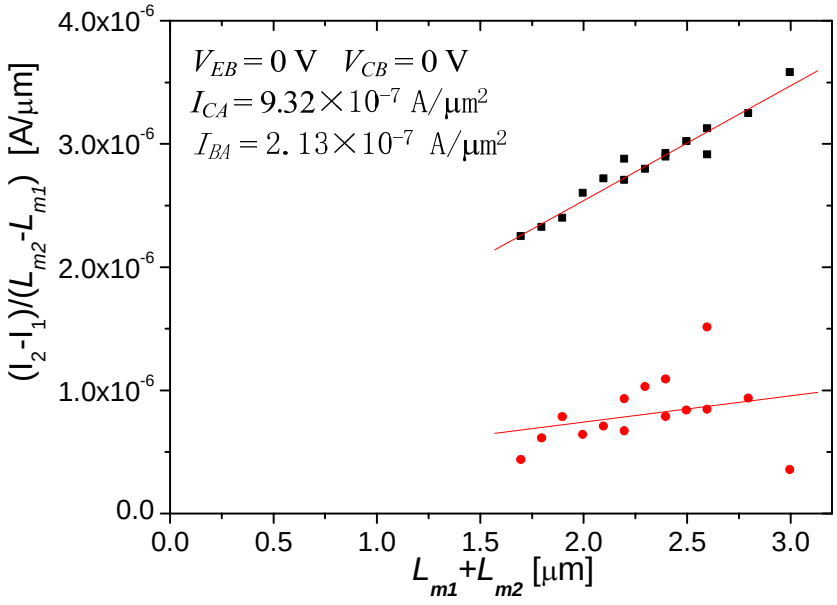

Figure 5.1 Extraction of area current density of collect current and base current with the bias that $V_{CB}=0$ V, $V_{EB}=0.7$ V.

Table 5.1 Extracted area current density of I_C and I_B

V_{CB} (V)	V_{EB} (V)	$I_{C\,A}$ (A/μm^2)	I_{BA} (A/μm^2)
0	0.50	$5.93\cdot10^{-10}$	$2.04\cdot10^{-10}$
0	0.52	$1.24\cdot10^{-9}$	$4.22\cdot10^{-10}$
0	0.54	$2.61\cdot10^{-9}$	$8.80\cdot10^{-10}$
0	0.56	$5.50\cdot10^{-9}$	$1.82\cdot10^{-9}$
0	0.58	$1.15\cdot10^{-8}$	$3.55\cdot10^{-9}$
0	0.60	$2.39\cdot10^{-8}$	$7.25\cdot10^{-9}$
0	0.62	$5.11\cdot10^{-8}$	$1.43\cdot10^{-8}$
0	0.64	$1.07\cdot10^{-7}$	$2.95\cdot10^{-8}$
0	0.66	$2.21\cdot10^{-7}$	$5.75\cdot10^{-8}$
0	0.68	$4.64\cdot10^{-7}$	$1.12\cdot10^{-7}$

5.2 Process and device simulation using Tsuprem4 and Medici [5,6]

Depending on the fabrication process of the p^+-n-p bipolar devices with Al doped SPE emitter, 1-D Tsuprem4 process simulation is implemented to abtain the doping profiles through the base region and the collector region of the p^+-n-p bipolar device. SIMS technique has been applied for the profiling of the SPE silicon region, and it is found that the Al doped SPE silicon is uniformly doped at around $1\cdot10^{19}$ cm^{-3} and the doping transition at the interface with the substrate is abrupt. However, SIMS can only tell the chemical doping concentration, from sheet resistance measurement, the active doping profile in the SPE emitter region is about $1\cdot10^{18}$ cm^{-3} [2].

During Medici simulations, the emitter is uniformly doped at $1\cdot10^{18}$ cm^{-3}, the doping profiles of the collector region and the base region are imported from Tsuprem4. Figure 5.2 shows the doping profile for the Medici simulation of the p^+-n-p bipolar and the carrier profiles at thermal equilibrium simulated by using Medici. In order to save the number of nodes in the simulated mesh, the substrate depth is set to be 2 μm. What is more, a thin layer at the bottom of collector region is highly doped to obtain an ohmic contact. The area of the Medici simulated emitter junction is set to be 1 μm $\times$1 μm, so the 1-D Medici simulated values of I_C and I_B are in fact the area current density and defined as I_{C_simu} and I_{B_simu} respectively.

During 1-D Medici device simulations, the surface recombination velocity and minority carrier lifetime are modulated to obtain different Gummel plots. Then the

simulated Gummel plots are compared to the extracted Gummel plot of area current density. It is found that good fitting can be achieved when the surface recombination velocity is between $7 \cdot 10^5$ cm/s and $1.2 \cdot 10^6$ cm/s. For the estimation of the minority carrier lifetime, the surface recombination velocity was fixed at $9 \cdot 10^5$ cm/s, and τ is modulated to obtain good fitting between Medici simulated Gummel plot and the extracted Gummel plot of area current density. One of the good fittings between the simulated Gummel plot and the extracted Gummel plot of area current density is shown in Figure 5.3.

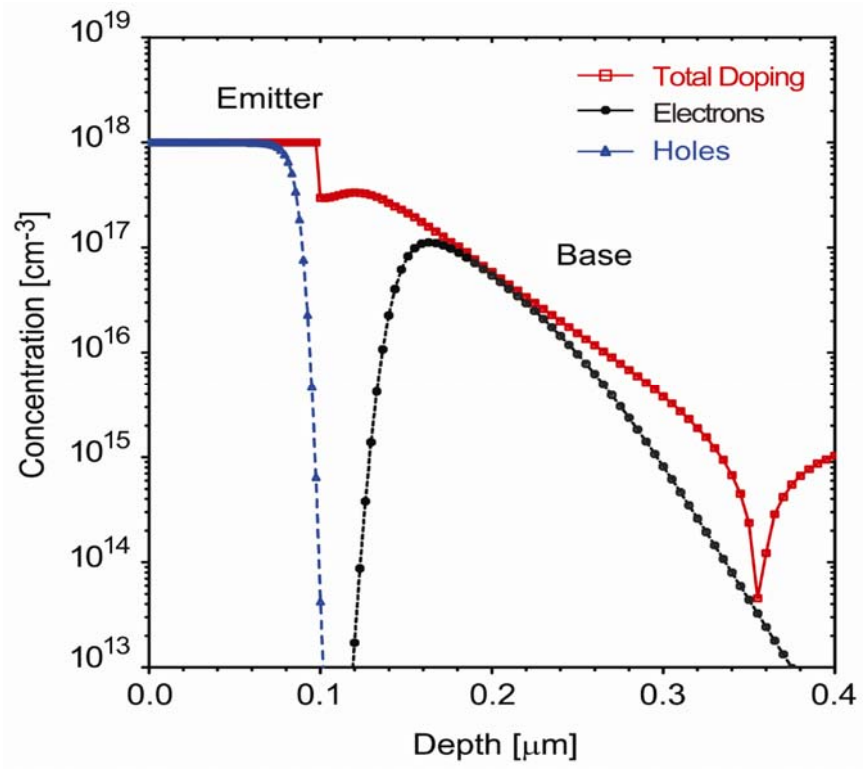

Figure 5.2 Tsuprem4 simulated doping profile and Medici simulated carriers profiles at thermal equilibrium.

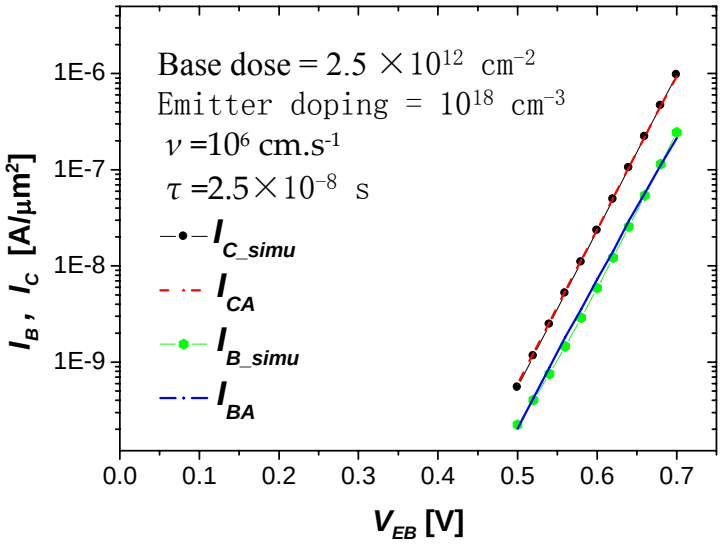

Figure 5.3. Fitting between simulated and extracted collector and base current density with base dose is $2.5 \cdot 10^{12}$ atoms/cm^2, the emitter doping is $1 \cdot 10^{18}$ /cm^{-3}, the depth of emitter is 0.1 μm, the surface recombination velocity is $1 \cdot 10^6$ cm/s, the minority carrier lifetime is $2 \cdot 10^{-8}$ s, the substrate depth is 2 μm

In summary, the surface recombination velocity at the interface of the Al-doped SPE emitter contact has been evaluated to be in the range of $7 \cdot 10^5$ cm/s and $1.2 \cdot 10^6$ cm/s which is comaparable to the normal value. The Minority carrier lifetime is about $2–3 \cdot 10^{-8}$ s, which would be expected for a B-doped high-quality monocrystalline Si.

Reference

[1] Yann Civale, Lis K. Nanver, Peter Hadley, Egbert J. G. Goudena, and Hugo Schellevis, “Sub-500 ◦C Solid-Phase Epitaxy of Ultra-Abrupt p$^+$-Silicon Elevated Contacts and Diodes,” in IEEE Electron Device Lett., vol. 27, no. 5, pp. 341 343, 2006.

[2] Yann Civale, Lis K. Nanve, and Hugo Schellevis, “Selective Solid-Phase Silicon Epitaxy of p+Aluminum-Doped Contacts for Nanoscale Devices,” in IEEE Trans. NanoTechn., vol. 6, no. 2, pp. 196 200, 2007.

[3] Yann Civale, Cuiqin Xu, Gianpaolo Lorito, Lis K. Nanver, Ramses van der Toorn, “Evaluation of Al-doped SPE ultrashallow P+N Junctions for use as PNP SiGe HBT Emitters,” International Workshop on Junction Technology, 2008, Shanghai, China,

pp. 97−100.
[4] P.A.H.Hart, “Bipolar and bipolar-MOS integration”, Elsevier, 1994
[5] http://www.synopsys.com
[6] http://www.avanticorp.com

6 Conclusions and Recommendations

6.1 Conclusions

The goal of the work presented in this thesis has been to develop a novel *C-V* measurement technique to extract the doping profiles of ultra-shallow junctions. This is done by extracting e.g. the p^+ doping profile of a p^+-n diode by combining the $C(V_R)$ relationships of a p^+-n and an n-Schottky diode with the same n profile. It has been demonstrated by analytical calculations and Medici simulations that it is possible to accurately extract the ultra-shallow profile if a stepped n doping profile is used. The principle of operation and the simulation results of this method are discussed in detail. The main conclusions of this thesis are:

Successful estimation of the doping profile on the p side of a p-n diode is possible with the knowledge of its $C(V_R)$ relationship, the doping profile on the other side and the position of the boundary of the depletion region to the neutral n region at thermal equilibrium (x_{n0}).

The position of the edge of the depletion region (x_{n0}) is a crucial parameter for the estimation of the doping profile in the p region of a p^+-n diode. Generally speaking, x_{n0} is not known and cannot be exactly determined.

If the doping profile in the n region is uniform, even with an incorrect value of x_{n0}, the doping gradient in the p^+ region can be accurately calculated. However, the exact position (depth) information of the p^+ region is not possible to estimate. What is more, it is not possible to profile deep into the p with the uniform profile.

带格式的：上标

带格式的：上标

It is shown that a p^+-n diode with a stepped n profile creates a specific *C-V* relationship which incorporates unusual features of the step-like n profile. In this case, attempting the extraction with a wrong assumption of x_{n0} results in an impossible p-profile. It is demonstrated that therefore by using different assumptions of x_{n0} a very small range of x_{n0} values results in a theoretically possible p^+ profile. As the range of x_{n0} is small, for all values of x_{n0} from that range, the extracted possible p^+ profiles fall also within a small range and therefore the p^+ can be regarded as accurately calculated.

6.2 Recommendations

The future work about the novel *C-V* profiling of ultra-shallow junctions by using a stepped n buried layer should be directed towards the optimization of the n profile in the measurement structures.

To optimize the breakdown voltage, p^+-n^--p^--n-n^+ and Schottky-n^--p^--n-n^+ structure is supposed.

To optimize the accuracy of results estimation and minimize the interval of x_{n0_assume}, optimized design of the stepped doping profile in the n region is necessary. The novel profiling method would work also for test structures with non-monotonic buried n layer.

To optimize the fabrication of measurement structures, the simplest n buried layer is appreciated. It is possible that good results can be achieved with only one abrupt change in the n profile.

To optimize the robustness of the fabrication, an n profile that can tolerate a high thermal budget is desired.

List of Symbols and Abbreviations

A: Area (cm^2)
BJT: Bipolar-junction transistor
C: Capacitance (F)
C_j: Junction capacitance per unit area (F/cm^2)
C-V: Capacitance versus voltage
DIMES: Delft Institute of Microsystems and Nanoelectronics
e: Elementary charge (C)
E: Electric field (V/cm)
ECV: Electrochemical capacitance-voltage
E_{Fi}: Intrinsic Fermi energy level (eV)
E_{Fs}: Fermi energy level of semiconductor (eV)
E_{Fm}: Fermi energy level of metal (eV)
$p_{\_simu}$: Simulated hole profile (cm^{-3})
$n_{\_simu}$: Simulated electron profile (cm^{-3})
I_B: Base current (A)
I_C: Collector current (A)
I_A: Area-proportional current density component (A/cm^2)
I_P: Perimeter-proportional current density component (A/cm)
I_K: Corner current component (A)
ITRS: International Technology Roadmap for Semiconductors
L: Side length of a square device (cm)
L_m: Nominal size of the side length of a square device
MOSFET: Metal oxide semiconductor field effect transistor
N_a: Density of acceptor impurity atoms (cm^{-3})
N_{a_esti}: Estimated acceptor concentration (cm^{-3})
N_{a_simu}: Simulated acceptor concentration (cm^{-3})
N_d: Density of donor impurity atoms (cm^{-3})
N_B: Doping concentration in the low doped region of an asymmetrical p-n junction (cm^{-3})
n_i: Intrinsic concentration (cm^{-3})
P: Perimeter (cm)
Q: Charge (C)
Q': Charge per unit area (C/cm^2)
RBS: Rutherford backscattering
SIMS: Secondary ion mass spectrometry
SRP: Spreading resistance profiling
S/D : Soure and drain
T: Temperature (K)

V: Potential (V)
V_{bi}: Built-in potential barrier (V)
V_{CB} Collector-base voltage (V)
V_{EB} Emitter-base voltage (V)
V_R: Reverse applied voltage (V)
V_T: Total potential drop across a p-n diode (V)
W: Total space charge width (cm)
x_{n0}: The position of the boundary of the depletion region to the neutral n region at thermal equilibrium (cm)
x_{p0}: The position of the boundary of the depletion region to the neutral p region at thermal equilibrium (cm)
x_{n0_assume}: Assumed value of x_{n0} (cm)
x_{n0_real}: Real value of x_{n0} (cm)
δx_{n0}: Difference between x_{n0_assume} and x_{n0_real} (cm)
x_{n_esti}: Estimated position of the boundary of the depletion region of the n region (cm)
x_{p_esti}: Estimated position of the boundary of the depletion region of the p region (cm)
ρ: Volume charge density (C/cm^3)
ϕ: Electric potential (V)
n: Electron concentration (cm^{-3})
p: Hole concentration (cm^{-3})
ε_s: Permittivity of a semiconductor (F/cm)

Acknowledgements

In the first place, I would like to thank Prof. Lis Nanver and Miloš Popadić for their support, encouragement and priceless help through this thesis. Also, I would like to thank Dr. Ramses van der Toorn, Yann Civale and Gianpaolo Lorito for their patient help. In particular, I would like to thank Francesco Sarubbi, Lei Gu, Luigi La Spina, Amir Sammak, whose personal and professional advices and help are invaluable.

Special thanks to Professor Guo-Ping Ru for his assistance, encouragement, understanding and consideration.

Furthermore, I would like to express my gratitude to DIMES IC Technology Group for their assistance with the processing.

I would like to thank Peter J.F. Swart and Sebastiaan Maas for their assistance with the measurements. Wim Tiwon and Rino Martillia are appreciated for their help with the computer support. Also, René van Swaaij, Rob Peeters, and Marian Roozenburg-de Bree are appreciated for their assistance and guidance with my study and work at TU-Delft.

I would like to thank my roommates, Danqing Liu, Theo Verhaar, Jun Hao and Faruk Krečinić for the harmonious working environment. Also, I would like to thank all my friends in Delft, you make my life here happier. I will always remember the happy tours and evenings.

Also, I would like to thank my friends in China, I have enjoyed the great friendship with you which does not depend on the distance between us. Special gratitude to Jing Wan, your understanding and support have always accompanied me.

In the end, I would like to thank my family for their love, encouragement and support. Special thanks to my brothers and sisters in law for their fealty, dedication and the happiness brought to the family.